Journal of Natural Gas Science and Engineering 101 (2022) 104507

Contents lists available at ScienceDirect

Journal of Natural Gas Science and Engineering

journal homepage: www.elsevier.com/locate/jngse

Integrated geophysical analysis of the Sembar Formation, Central Indus Basin, as an unconventional resource

Aamir Ali [a], Tiago M. Alves [b,*], Yawar Amin [a]

[a] Department of Earth Sciences, Quaid-i-Azam University, 45320, Islamabad, Pakistan
[b] 3D Seismic Lab, School of Earth and Ocean Sciences, Cardiff, University, CF10 3AT, United Kingdom

ARTICLE INFO

Keywords:
South Asia
Shale oil and gas
Fuel energy
Seismic inversion
TOC

ABSTRACT

The ever-increasing demand for new energy sources witnessed at present is leading to a shortage of oil and gas resources throughout the world. At the same time, polluting energy sources such as coal are being gradually replaced by gas, new fuel types and electricity produced by renewable methods. Unconventional shale gas reserves, relying on the presence of substantial volumes of good quality, thermally mature organic matter, are therefore crucial in shaping the economic future of multiple regions in the world. Using seismic reflection data to estimate Total Organic Carbon (*TOC*) in the underexplored Sembar Formation of the Qadirpur Area, Central Indus Basin, this study investigates the potential of a new unconventional resource in Pakistan. We estimate *TOC* based on well-log data using Passey's Δ Log R, Schmoker's, and Schwarzkopf's methods. In a second stage, thermal maturity modelling was carried out for the formations encountered in Well Qadirpur Deep-01, while focusing primarily on the Sembar Formation. Petrophysical and petroelastic properties were determined and cross-plotted to identify potential zones favourable to hydraulic fracturing. The results show calculated *TOC* values ranging from 2 to 4 wt% based on the multiple methods indicated above, proving that the Sembar Formation is a good to excellent unconventional oil gas play. Thermal maturity modelling further confirms that the organic matter in the Sembar Formation is mature. Our seismic based spatial distribution indicates that *TOC* values are particularly favourable in the lower part of the formation, which is also prone to hydraulic fracturing based on its petroelastic evaluation. This study presents a valid approach to characterise source-rock potential in sedimentary basins throughout South Asia and around the world.

1. Introduction

Shale is a fine-grained sedimentary rock that often comprises volumes of organic matter considered essential to form a hydrocarbon source rock (Ali et al., 2017; Gao et al., 2020). Unconventional resources such as tight gas, coal-bed methane and shale oil are able to contain (trap) significant amounts of hydrocarbons in particular geological settings, with shale gas and oil recording the greatest potential and significance in South Asia's sedimentary basins (Sunjay, 2011). Tight shale gas and oil fields have become important in the last few decades as a complementary source of energy, while renewable, hydrogen and geothermal sources are being investigated around the world (Jarvie et al., 2007; Jarvie, 2012; Yu et al., 2017). In order to classify such fields, shales and mudstones with adequate amounts of organic matter are usually investigated as potential source rocks, whereas rocks with a low organic content qualify as non-source rock, regardless of their lithology (Passey et al., 1990).

Estimates of Total Organic Carbon (*TOC)* are considered vital for shale reservoir characterisation (Yu et al., 2017). However, and in contrast to conventional gas reservoirs, a shale formation's inadequate permeability, exceedingly low porosity, and restricted contact area with reservoir rocks, can often hinder the economic production of such shaley units (Eshkalak et al., 2014). Reservoir stimulation by means of hydraulic fracturing and frequent use of horizontal wells to enhance production rates are also pivotal for an economic production in such rocks (Glorioso, 2012). The identification and mapping of the lateral and vertical extents of source rocks, using seismic and well data, lays the foundations of *TOC* evaluation in unconventional oil and gas fields (Løseth et al., 2011; Rezaee, 2015; Aziz et al., 2018). Various methods can be used to precisely estimate *TOC* at borehole, including the Δ log R (Passey et al., 1990), Schmoker (1981) and Schwarzkopf (1992) methods. To further examine shale resource potential, thermal maturity

* Corresponding author.
E-mail address: alvest@cardiff.ac.uk (T.M. Alves).

https://doi.org/10.1016/j.jngse.2022.104507
Received 14 July 2021; Received in revised form 6 February 2022; Accepted 4 March 2022
Available online 10 March 2022

models based on detailed analyses of a basin's burial and temperature histories is essential for evaluation of organic matter maturity in 4D (time and space) (Rybach, 1986; Wood, 1988; Blackwell and Richards, 2004; Wandrey et al., 2004; Rickman et al., 2008; Waples et al., 2010; Rezaee, 2015; Ali et al., 2017). Whilst *TOC* analyses comprise the *de facto* first step towards understanding the hydrocarbon potential of unconventional fields, the low effective porosity in shale source hinders hydrocarbon extraction even after drilling is completed. The identification of possible zones favourable to hydraulic fracturing is therefore undertaken in second stage by estimating the petroelastic properties of source rocks (Ali et al., 2017). Parameters such as the Brittle Shale Index (*B*), Young's Modulus (*E*) and Poisson's Ratio (*PR*) are the principal petroelastic parameters controlled by the presence of organic matter and can be used to point out key locations for hydraulic fracking. In parallel, regional *TOC* distributions can also be confidently mapped at a distance from well control points on reservoir scale with the help of detailed well-log data ties to seismic data (Løseth et al., 2011; Rezaee, 2015; Aziz et al., 2018).

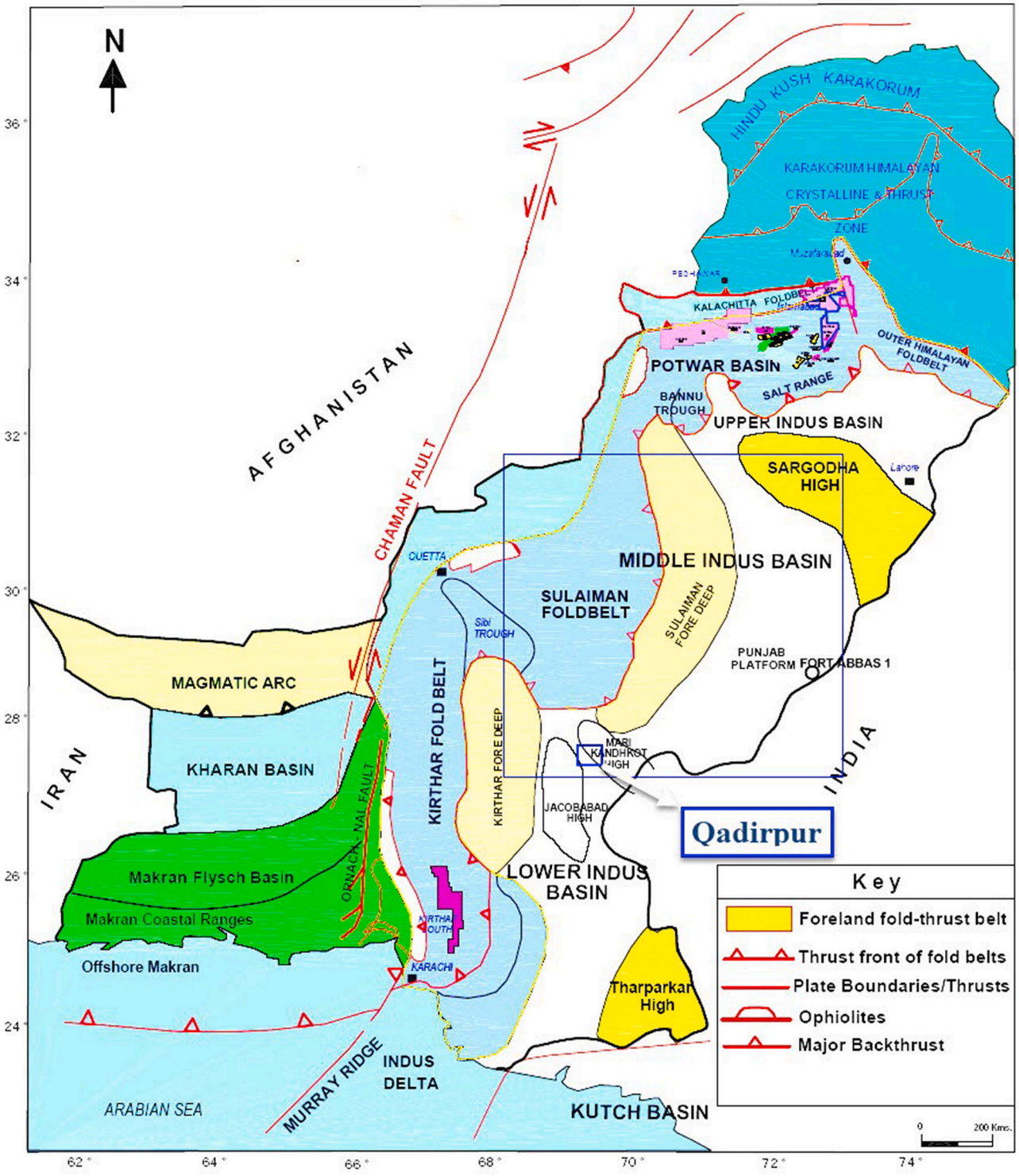

Fig. 1. Tectonic map displaying major sedimentary basins in Pakistan and the study area in this work (modified from Asim et al., 2014; Ali et al., 2019).

The objective of this work concerns the evaluation of unconventional hydrocarbon resources in the Sembar Formation of the Qadirpur area, Central Indus Basin, Pakistan (Fig. 1). It concerns the comprehensive spatial mapping of *TOC* content in the area of interest by means of seismic and well log data, and petroelastic analyses. Although a few Pakistan basins have been evaluated for shale oil and gas according to the EIA (2013) report, a detailed assessment of the Southern Indus Basin in terms of its shale gas potential is still missing (Sheikh and Giao, 2017). This is an important caveat, knowing that US Energy Information Administration recognised, for Pakistan alone, total reserves of 586 TCF of shale gas with a recoverable 100–105 TCF (EIA, 2013). This study investigates, for the first time, the unconventional potential of the Qadirpur area by focusing on the Sembar Formation. The Qadirpur area has been vigorously exploited in terms of its conventional carbonate reservoirs (Ali et al., 2019), but is lacking an assessment of its unconventional sources. In summary, this work aims to address the following research questions:

a) Does the Sembar Formation have enough *TOC* value to act as an unconventional resource?
b) Does the Sembar Formation have enough thermal maturity to be productive?

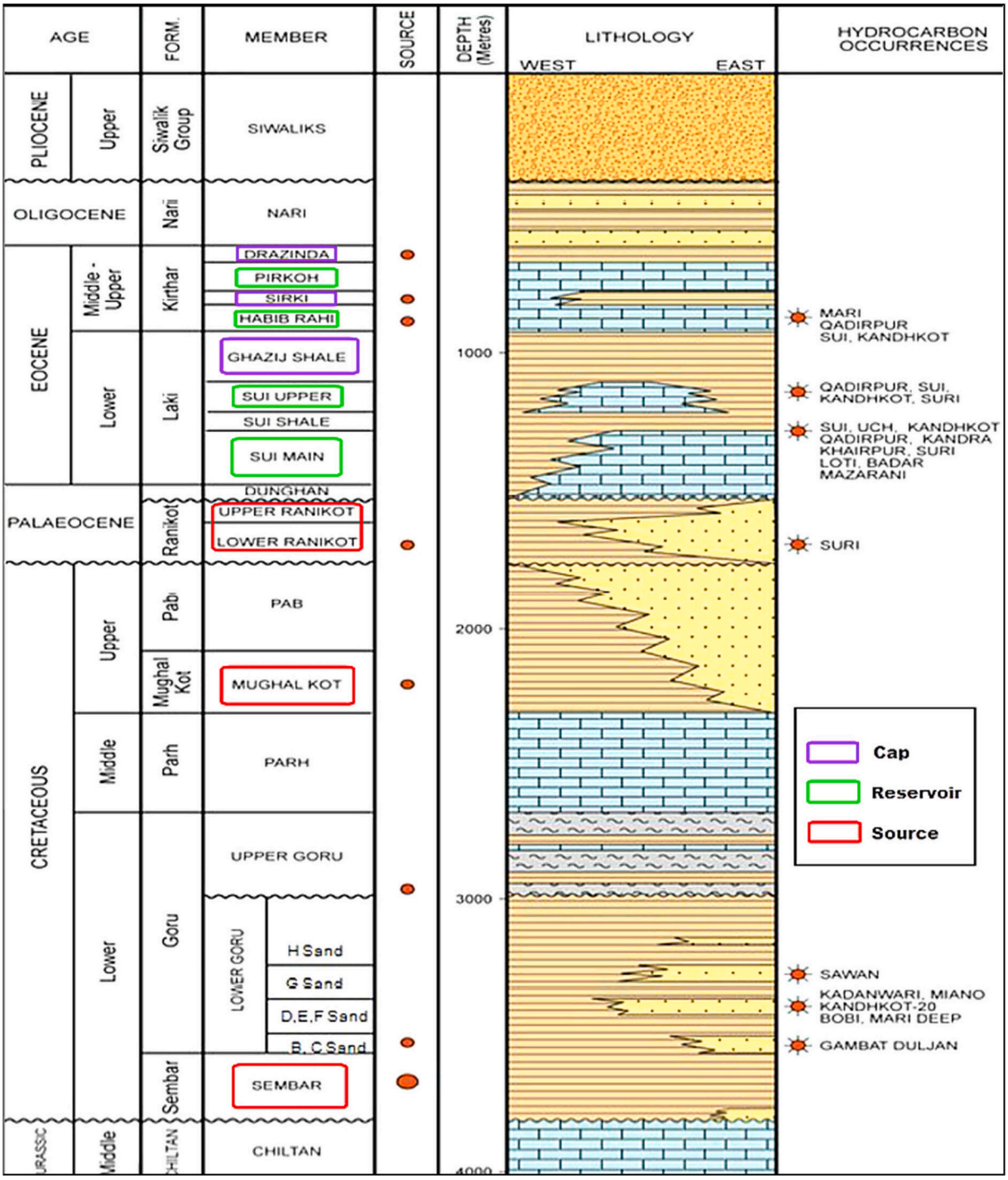

Fig. 2. Stratigraphic panel for the Central Indus Basin, Qadirpur locality (modified by Alam et al., 2002; Ali et al., 2005; Ahmed et al., 2013; Abbasi et al., 2014; Ali et al., 2019).

c) Is the Sembar Formation prone to economic hydraulic fracturing?

2. Geological setting

The Qadirpur area, the focus of this study, extends through 820 km^2 across the Sindh Province, Pakistan (Ali et al., 2005). It is located in the southern part of the Central Indus Basin (Fig. 1). Extensional tectonics initiated in the Cretaceous influenced the formation of structures favourable for the accumulation of oil and gas in the region (Milan and Rodgers, 1993; Ali et al., 2019).

Within the Central Indus Basin, the oldest units drilled by exploration wells are Upper Triassic in age. An erosional period controlled the deposition of the Sembar Formation, the focus of this study, which is relatively younger towards the west. As a result, the probability of hydrocarbon presence within the Sembar Formation is low towards the Kirthar Mountains to the west of the study area, but accumulations are noted south and southeast of the study area, still within the Sindh Province (Eickhoff and Alam, 1991; Ali et al., 2018). Importantly, the boundary between the Lower Goru Sand Member acting as a conventional reservoir and the Sembar Formation is marked by a regional unconformity (Ahmad et al., 2011).

The Central Indus Basin is currently the largest hydrocarbon producing Basin in Pakistan (Khan et al., 2016). The main conventional reservoirs in the Central Indus Basin are Sui Main Limestone and the Sui Upper Limestone (Fig. 2). The Sembar Formation has a variable lithological composition in different areas (Ahmad et al., 2011; Aziz et al., 2018). Its average lithological composition comprises 42% Quartz, 47% Clay, 10% Calcite and 1% Pyrite (Ahmad et al., 2011; Aziz et al., 2018). In the study area, the Cretaceous shales in the Sembar Formation form the main regional-scale source rocks, with the upper Cretaceous Mughalkot shale and the Paleocene Ranikot Formation also generating hydrocarbons at a local scale (Ali et al., 2019) (Fig. 2). The Sembar Formation is chiefly composed of shale with minor patchy intercalations of siltstone and sandstone (Iqbal and Shah, 1980; Raza et al., 1990; Aziz et al., 2018). Within the Central and Lower Indus Basins, the Sembar Formation is historically considered as the most favourable when it comes to source-rock thickness, *TOC* presence and thermal maturation (Wandrey et al., 2004; Aziz et al., 2018).

3. Data acquisition and methods

This work uses two-dimensional (2D) seismic lines, their navigation files, well header and wireline curves for Well Qadirpur Deep-01, which was chosen for being relatively deep, drilling sediment as old as the Jurassic (186 Ma) Chiltan Formation (Fig. 2). Thus, the Sembar Formation can be petro-physically analysed using this well. The acquisition and processing parameters are provided in Table 1. The base map displaying the location and orientation of seismic lines and wells used in this work is given in Fig. 3. The frequency range of the seismic data is 10–55 Hz with the best resolution of the target depth occurring at a frequency range of 10–35 Hz.

Wireline data used in this work include porosity, Resistivity (LLD) and Gamma-Ray (GR) curves for hydrocarbon-play identification, and potential *TOC* calculations using the Passey's Δ Log R technique (Passey et al., 1990), the Schmoker's technique (Schmoker, 1979) and the Schwarzkopf's method (Schwarzkopf, 1992). An unconventional resource, despite excellent *TOC* content, is only as good as its potential to be fractured (Shrestha et al., 2017). Petroelastic and petrophysical properties were therefore calculated using the available wireline data, and potential zones for hydraulic fracturing were determined for the Sembar Formation on the basis of its estimated *BSI*, *E*, and *PR* values. Thermal maturity modelling was carried out to evaluate organic maturity in the Sembar Formation based on temperature history, burial history, and time temperature index.

A combination of calibrated well-based rock physics models and seismic data can provide reliable models at reservoir scale for units such as the Sembar Formation. Hence, values extracted from a Simulated Annealing Inversion (*RSAI*) section were plotted against *TOC* obtained from Passey's, Schmoker's, and Schwarzkopf's methodologies after upscaling the log data. A regression line was calculated and *TOC* sections were developed using the straight line (regression) equations for each methodology indicated above. A complete workflow for this study is presented in Fig. 4.

Table 1
Acquisition and processing parameters of the seismic data used in this work.

Acquisition Parameters			
Source		Field parameters	
Energy Source	Dynamite	Format	SEG-D (DMUX)
Charge Pattern	1 Hole	Field Sampling Interval	2 ms
Average Charge Size	3 Kg	Record length	5 Seconds
Average Shot Depth	21 Meters	No. of Data Traces	240
S.P. Interval	50 Meters	Group Interval	25 Meters
Processing Parameters			
Demultiplex	Bandpass Filter	Residual Statics Correction	Time Variant Filter
Preprocessor	Surface Consistent Deconvolution	Velocity Analysis (CVA)	Random Noise Attenuation
Geometrical Spreading Compensation	CDP Sort	Stack	RMS Gain
Exponential Gain	Velocity Analysis (CVA)	Finite Difference Migration	–
FK Dipfilter	Normal Moveout Correction	Multichannel Coherency Filter (MCCF)	–

Well Name	Elevation (KB (m))	Total Depth (m)	Status
Qadirpur Deep-01	78	4694.0	Oil and Gas Well

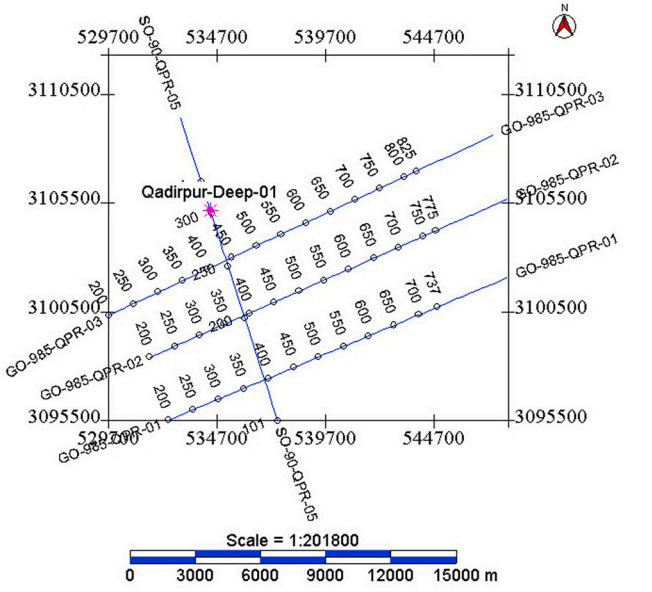

Fig. 3. Base map of the Qadirpur Area showing a NW-SE oriented strike line, three NE-SW oriented dip lines and Qadirpur Deep-01.

3.1. Demarcation of the Sembar Formation

The base and top of the Sembar Formation were first interpreted on a NW-SE oriented seismic line through the help of a synthetic seismogram

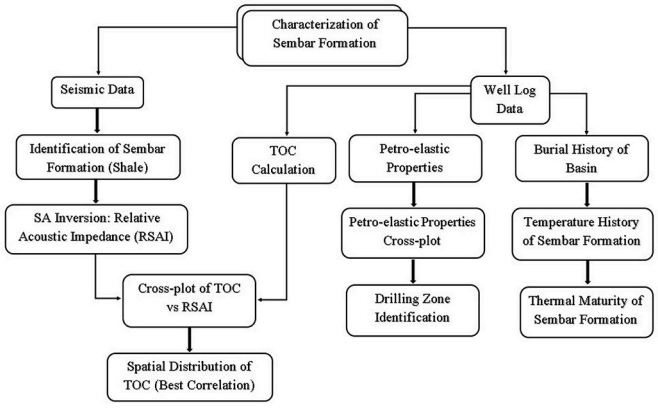

Fig. 4. Workflow followed in this study to characterise the Sembar Formation.

generated using well-log data (Fig. 5). Faults were interpreted and time and depth contour maps were generated to determine the lateral and vertical trend of the Sembar Formation throughout the study area (Figs. 6 and 7). An isopach map for the Sembar Formation was generated to document its thickness throughout the study area (Fig. 8).

3.2. TOC estimates

The Δ Log R method was developed by Exxon/Esso and has been successful in determining *TOC* at well locations around the world (Passey et al., 1990). Even though new techniques offer the advantage of determining organic content directly, the Δ Log R method has the advantage of working effectively in clastic as well as carbonate source rocks (Passey et al., 1990). The technique requires the superimposition of LLD curves against one of the three 'basic' porosity logs, Neutron (NPHI), Density (RHOB) and Sonic (DT) log, after a scale adjustment is applied to the data (Passey et al., 1990). A logarithmic LLD log is therefore plotted against one of the linearly scaled porosity logs (Rider, 2002), but since borehole conditions can affect the NPHI and DT logs, it is better to plot the LLD curve against the DT log for more accurate results (Liu et al., 2012). After the curves are superimposed, a baseline is documented within a fine-grained, non-source interval (Passey et al., 1990). The demarcation of a baseline requires professional experience since the accuracy of the results varies drastically with differing approaches.

Another variable required to estimate *TOC* using Passey's Δ Log R method is the Level of Metamorphism, also known as Level of Maturity (*LOM*), which is estimated on the basis of the vitrinite reflectance method (Tissot and Welte, 1978; Robert, 1988; Hunt et al., 1996; Galasso et al., 2019). Using Formation temperature for the Sembar Formation in Well Qadirpur Deep-01 (Table 2), vitrinite reflectance (*Ro*) for the Sembar Formation was determined through the graphical method in Fig. 9. The chemical and physical change which a rock undergoes due to increasing burial temperature and overburden pressure is termed as *rank* (Hood et al., 1975). The *LOM* is a unitless property that can be determined through a number of methods. One such method is the graphical method which plots *Ro* values for a specific source rock on the horizontal (x) axis against the respective *LOM* values on the vertical (y) axis. For the Sembar Formation, the graph in Fig. 10 was developed based on data from Well Qadirpur Deep-01.

DT and LLD curves provide the best results in *TOC* estimates. First, the logs are scaled so that a specific interval of DT log equals one complete logarithmic cycle of LLD log. In this work, the wireline curves are scaled so that 100 μs/ft equals two logarithmic LLD cycles. The interval of superimposition is within the non-source rock at a depth of 4033 m marking the baseline. In the second stage, the separation between the two curves is determined; this separation is called the Δ Log R curve (Fig. A1). This curve is then used in the following equations to determine *TOC* curves for specific intervals (Passey et al., 1990):

$$\Delta LogR_{DT} = Log10\left(\frac{R}{R_{Baseline}}\right) + 0.02 \times (\Delta t - \Delta t_{Baseline}), \quad (1)$$

$$TOC_{DT} = \Delta LogR_{DT} \times 10^{(2.297 - 0.1688 \times LOM)}, \quad (2)$$

where, $\Delta LogR_{DT}$ represents the separation between DT and LLD curves, R are the resistivity values (in Ohms · meter) from the LLD log. In Equation (1), $R_{Baseline}$ is the baseline value for the LLD curve equivalent to the DT baseline value, Δt reflects the transit-time values from the DT log (in μsec/ft). In parallel, $\Delta t_{Baseline}$ is the baseline value for the DT curve corresponding to the LLD baseline value. In this work, 0.02 is the scaling factor which was determined through equating 50 μs/ft to 1 Ωm, therefore indicating that 1 μs/ft is equal to 1/50 Ωm, which in turn is equal to 0.02 Ωm. The parameter TOC_{DT} represents the organic matter values in percentage weight (wt%) calculated via the DT log, while *LOM* is the Level of Maturity. After establishing a baseline, specified baseline values for $R_{Baseline}$ and $\Delta t_{Baseline}$ are used throughout the borehole to determine the needed *TOC* values (Passey et al., 1990). The Passey's Δ

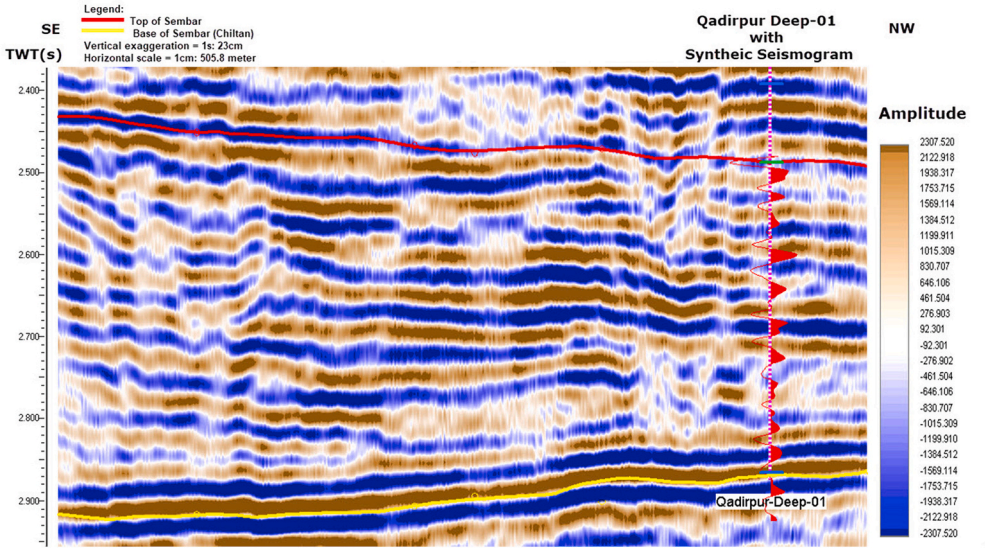

Fig. 5. Seismic line SO-90-QPR-05 with synthetic seismogram superimposed on the section.

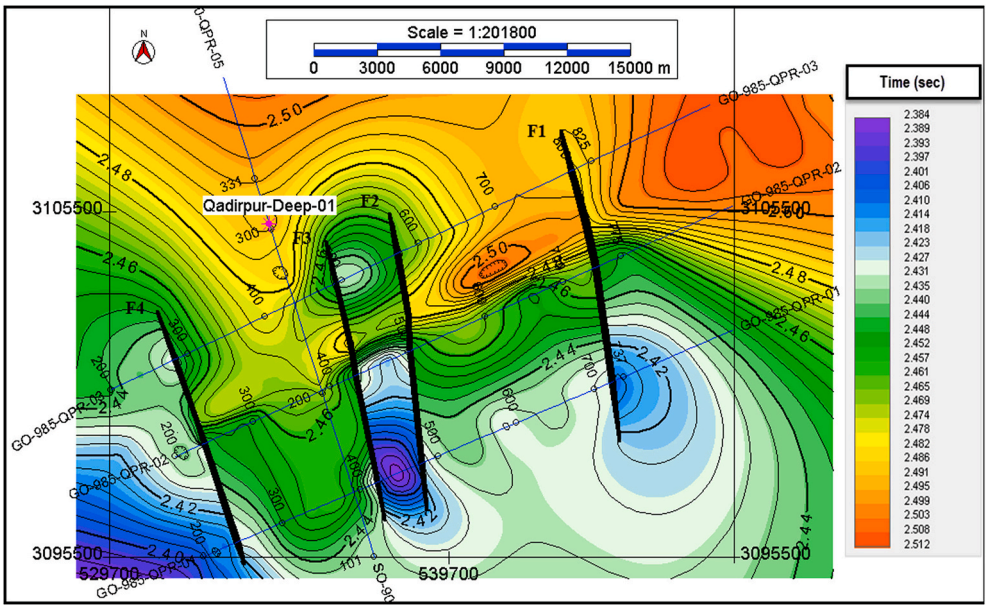

Fig. 6. Time-contour map of the Sembar Formation following a contour interval of 0.004 s.

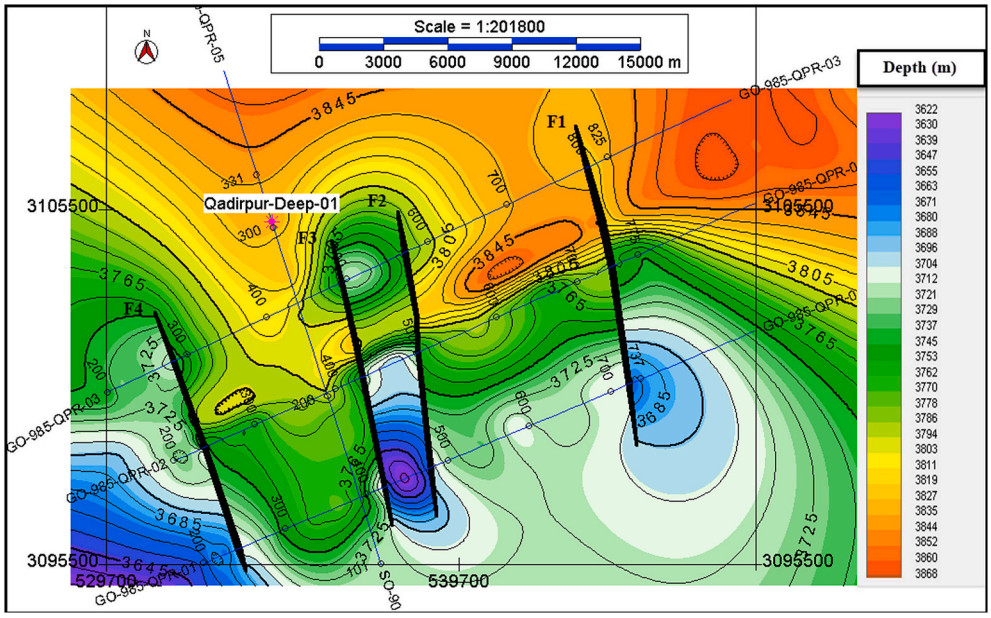

Fig. 7. Depth-contour map of the Sembar Formation following a contour interval of 10 m.

Log R technique for DT and LLD logs applied to Well Qadirpur Deep-01 is shown in Fig. A1.

Another way to use Passey's Δ Log R method is by superimposing the LLD log over RHOB. In the Well Qadirpur Deep-01, one logarithmic LLD cycle equals 0.4 g/cm^3 in the RHOB log (1 Ωm equals 0.4 g/cm^3). The equations used to calculate *TOC* using LLD and RHOB logs are based on Passey et al. (1990) such as:

$$\Delta\, LogR_{RHOB} = Log10\left(\frac{R}{R_{Baseline}}\right) - 2.5 \times (\rho_b - \rho_{Baseline}) \quad (3)$$

$$TOC_{RHOB} = \Delta LogR_{RHOB} \times 10^{(2.297-0.1688 \times LOM)} \quad (4)$$

where, $\Delta LogR_{RHOB}$ reflects the separation between RHOB and LLD logs, R represent the LLD log values in Ωm, and $R_{Baseline}$ is the baseline value for the LLD curve corresponding to the RHOB baseline value. In addition, ρ_b represents the bulk density values using RHOB curve (g/cm^3), and $\rho_{Baseline}$ is the RHOB baseline value corresponding to the LLD baseline value. The parameter TOC_D represents the *TOC* values in percentage weight (wt%) estimated with the help of the RHOB log, while *LOM* is the Level of Maturity. By applying the Passey's method to Well Qadirpur Deep – 01, *TOC* values were calculated as shown in Fig. A2.

Passey et al. (1990) proposed a relationship between NPHI and LLD log data to determine *TOC* values. The scale factor used to superimpose the two curves (NPHI against LLD) is one logarithmic LLD cycle to 0.25 v/v (1 Ωm equals 0.25 v/v). Relevant equations from Passey et al. (1990) are given as follows:

$$\Delta LogR_{NPHI} = Log10\left(\frac{R}{R_{Baseline}}\right) + 4.0 \times (\varnothing N - \varnothing N_{Baseline}) \quad (5)$$

$$TOC_{NPHI} = \Delta LogR_{NPHI} \times 10^{(2.297-0.1688 \times LOM)} \quad (6)$$

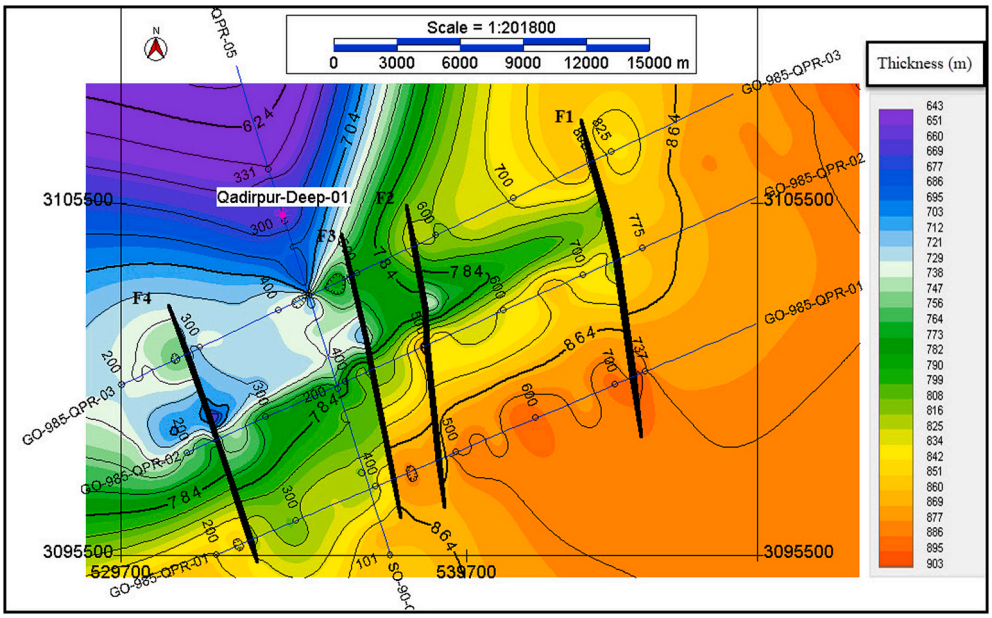

Fig. 8. Isopach map depicting the thickness of the Sembar Formation following a contour interval of 16 m.

Table 2
Depth, thickness and temperature of stratigraphic formations in the Qadirpur Area as encountered by Well Qadirpur Deep-01.

Formation	Age		Depth	Thickness	Temperature
		Ma	m	m	K
ALLUVIUM	Recent	1	0	95	306.15
UNCONFIRMITY		2			
PLIESTOCENE		3			
SIWALIKS	Pleistocene/ Pliocene	18	95	387	309.15
UNCONFIRMITY		23.5			
E. MIOCENE		29			
NARI	Miocene/ Oligocene	41	482	220	321.15
DRAZINDA	Middle Early Eocene	43	702	56	328.15
PIRKOH	Middle Early Eocene	45	758	109	330.15
SIRKI	Middle Early Eocene	47	867	46	333.7
HABIB RAHI	Middle Early Eocene	49	913	85	335.15
GHAZIJ	Middle Early Eocene	56	998	199	337.75
SUL	Middle Early Eocene	57	1197	58	340.95
Sui Shale	Middle Early Eocene	58	1255	51	345.95
SML	Middle Early Eocene	59	1306	143	347.55
DUNGHAN LST	Paleocene	61	1449	46	352.15
L RANIKOT	Paleocene	68	1495	71	353.55
UNCONFIRMITY		69.5		0	
L. CRETACEOUS		71			
PAB	Cretaceous	73	1566	239	355.85
FORT MUNRO	Cretaceous	74	1805	76	363.45
MUGHALKOT	Cretaceous	75	1881	287	365.85
PARH	Cretaceous	81	2168	179	374.95
UPPER GORU	Cretaceous	91	2347	739	380.65
LOWER GORU	Cretaceous	101	3086	824	404.15
SEMBAR	Cretaceous	165	3910	776	430.15
CHILTAN	Jurassic	186	4686	8	455.15

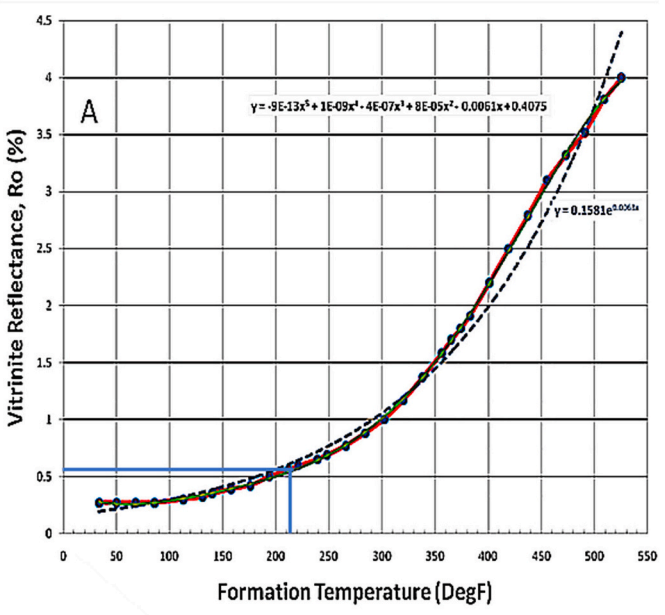

Fig. 9. Formation temperature and *Ro* Model modification after Hill et al. (2007) and Ehsan et al. (2016). *Ro* for the Sembar Formation in Well Qadirpur Deep – 01 well is estimated to be 0.55.

where, $\Delta LogR_{NPHI}$ represents the separation between the NPHI and LLD logs, $\varnothing N$ represents the NPHI log, $\varnothing N_{Baseline}$ is the baseline value for NPHI correlating with to LLD log's baseline value, R reflects the LLD log values (in Ohm · meter), and $R_{Baseline}$ is the LLD baseline value correlating with NPHI baseline value. In addition, TOC_N is *TOC* in percentage weight (wt%) extracted from the NPHI log, and *LOM* is the Level of Maturity. Data from Well Qadirpur Deep-01 return the results shown in Fig. A3 upon applying Equations (5) and (6).

Organic matter has a relatively lower density in comparison to the surrounding rocks, resulting in contrasts between the density of solid organic matter and the background matrix. *TOC* estimates using Schmoker's method show a positive linear correlation with the inverse of the RHOB log values (Schmoker, 1979):

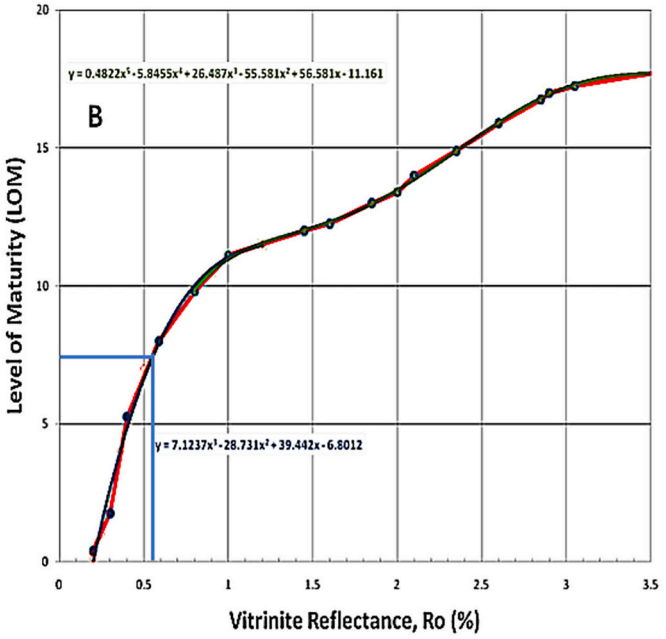

Fig. 10. *LOM* and *Ro* Model modification after Alyousuf et al. (2011) and Ehsan et al. (2016). From the graphical method it can be observed that the *LOM* value for the Sembar Formation varies from 7 to 8.

$$TOC = A^{*}\left(\frac{1}{\rho}\right) - B \tag{7}$$

where the constants A and B are determined on the basis of organic matter content and the density of the source rock. Its computation can also be undertaken by measuring the relative proportion of organic content vs. organic carbon. In Equation (7), ρ is the density taken from the RHOB log. The *TOC* is measured in weight percentage (wt%). After determining the above parameters A and B based on data acquired from Well Qadirpur Deep-01, Equation (7) can be simplified as follows:

$$TOC = \left(\frac{154.497}{\rho}\right) - 57.261 \tag{8}$$

where, ρ is the density of the source rock (taken from the RHOB log). The *TOC* values computed for Well Qadirpur Deep-01 using the Schmoker's method are shown in Fig. A4.

Schwarzkopf's (1992) method makes certain assumptions before estimating *TOC* values from wireline data: 1) non-source rock has an organically lean trend, and 2) source and non-source intervals have the same porosity and matrix density values. Similar assumptions and methods were also used by Myers and Jenkyns (1992) to determine *TOC*.

The porosity of non-source intervals is calculated using Equation (9). In Schwarzkopf's (1992) method, Equation (10) is used for estimation of kerogen type. After calculating the above-mentioned variables, *TOC* is determined using Equation (11) as follows:

$$\varnothing_{sat} = \frac{\rho_{ma} - \rho_{ns}}{\rho_{ma} - \rho_{fl}} \tag{9}$$

$$\varnothing_{ker} = \frac{\rho_{s} - \rho_{ns}}{\rho_{ker} - \rho_{ma}} \tag{10}$$

$$TOC = \frac{0.85 \times \rho_{ker} \times \varnothing_{ker}}{\rho_{ker} \times \varnothing_{ker} + \rho_{ma}\,(1 - \varnothing_{sat} - \varnothing_{ker})} \tag{11}$$

where, $\varnothing_{sat}$ represents in Equation (9) the water-filled porosity value of a rock, ρ_{ns} is the density of non-source strata (its average value taken from wireline. logs) in g/cm^3, ρ_s is the density of the source-rock interval (also taken from wireline from log) in g/cm^3. The parameter. $\rho_{ma} = 0.2.7$ g/cm^3 is the assumed density of mudrock, ρ_{fl} is the average water density, and $\varnothing_{ker}$ is the porosity for kerogen-packed source rocks.

DT logs can also be used to estimate *TOC* within a source interval, using a similar approach. The only problem is the comparatively lesser sensitivity of the DT travel time as compared to the RHOB log (Schwarzkopf, 1992). Furthermore, porosity and lithology types have a greater effect on the DT log when compared to the RHOB log (Meyer and Nederlof, 1984). The methodology used on Well Qadirpur Deep-01 provided the results illustrated in Fig. A5.

3.3. Thermal maturity evaluation

Thermal maturity can be modelled using wireline data based on the following methodology: 1) burial histories need to be interpreted in first stage for each stratigraphic unit taking unconformities and erosional events into account, 2) thermal conductivities for each stratigraphic unit should be estimated to reconstruct a basin's thermal history, and 3) kerogen maturation should be determined taking into account the types and ages of kerogen in a source rock (in this case, the Sembar Formation):

3.4. Burial history

The burial history of a basin is estimated based on the thickness, depth and temperature of each rock unit. Information from Well Qadirpur Deep-01 is given in Table 2. Three uplift episodes have been considered in our models based on the presence of regional unconformities. The thickness of the eroded successions has been estimated on the basis of the well's subsidence trend and the depositional ages of the drilled stratigraphic formations (Fig. A6).

3.5. Thermal history

Thermal (or temperature) history is estimated using Fourier's law of heat conduction, which is given by the following equation (Blackwell and Richards, 2004; Ali et al., 2017):

$$\Delta T = QL/K \tag{12}$$

where ΔT is the temperature gradient, Q is heat flow, L is the thickness of the stratigraphic formation of interest, and K is thermal conductivity. Using the difference in temperature for each paleo-depth of a specific formation (in this case, for the Sembar Formation) while keeping Q and

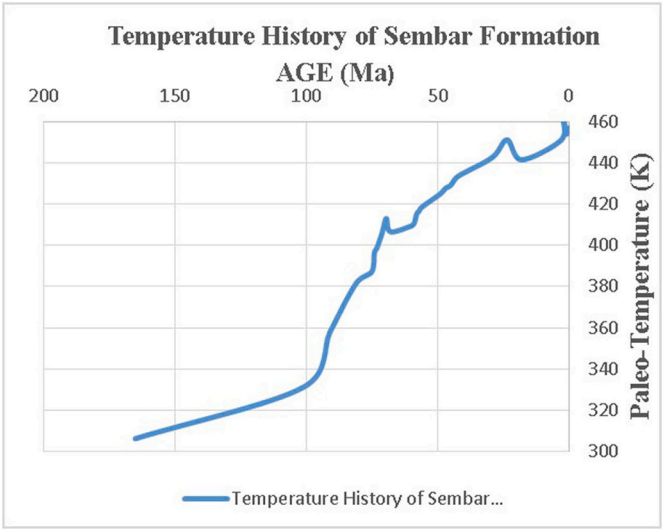

Fig. 11. Log based temperature history of the Sembar Formation for Well Qadirpur Deep–01.

K constant, the temperature history can be determined using the following relation given by Blackwell and Richards (2004):

$$T_n = T_0 + Q\left(\frac{L_1}{K_1} + \frac{L_2}{K_2} + \ldots + \frac{L_n}{K_n}\right) \tag{13}$$

where T_n is the temperature (K) at the base of a stratigraphic unit, T_0 is the average paleo-surface temperature (K). The heat flow for a stratigraphic unit can be estimated using the equation given by (Rybach, 1986):

$$Q = q + A_0 D \tag{14}$$

where, q and D, are constants. D is the paleo-depth for a specific stratigraphic formation and the value of q is generally taken to be 27 mW/m^2. The parameter A_0 is the heat generation value in W/m^3 and can be calculated utilizing GR log and the empirical relationship given by Bucker and Rybach (1996):

$$A_0 = 0.0158(GR - 0.8) \tag{15}$$

The values of Q (Equation (14)) and K (Equation (12)) for the Sembar Formation have been estimated as 0.0336 W/m^2 and 284.8802 W/m.K (1.042944 W/m°C), respectively. Estimates of paleo-surface temperatures (Figs. 11 and 12; Table 3) led to the development of the temperature history curve based on Equation (13).

3.6. Thermal maturity of organic matter

It is known since the mid-1960s that organic matter matures as the temperature and pressure exerted on a source rock increases with time (Habicht, 1964; Philippi, 1965; Hunt et al., 1991). In order to develop a relationship between maturity of the organic matter and temperature as a function of time, Wood (1988) derived a time temperature index using the Arrhenius equation (Hunt et al., 1991). The Arrhenius equation theoretically expresses the rate of a chemical reaction as depending on the square power of temperature (Connan, 1974; Wood, 1988). The pre-exponential factor A and the activation energy E are related to the time-dependent temperature index ($\sum TTI_{Arr}$) of a specific stratigraphic formation (Hunt et al., 1991; Wood, 2017; Ali et al., 2017) via Equation (16) below:

$$TTI_{Arr} = \frac{A(t_{n+1} - t_n)}{T_{n+1} - T_n}\left\{\left[\frac{RT_{n+1}^2}{E + 2RT_{n+1}}\exp\left(-\frac{E}{RT_{n+1}}\right)\right] - \left[\frac{RT_n^2}{E + 2RT_n}\exp\left(-\frac{E}{RT_n}\right)\right]\right\} \tag{16}$$

where TTI_{Arr} is time-dependent temperature index from time period t_n to t_{n+1} for a formation experiencing a temperature change from T_n to T_{n+1} (K), and the parameter R is gas constant (0.008314 kJ/mol · K). The values of A and E for the Sembar Formation were considered to be 5.45E+26 Ma^{-1} and 218 kJ/mol based on information in Wood (1988) and Wood (2017). In this work, a time-dependent temperature index was computed for the Sembar Formation using paleo-depth data, as shown in Fig. 13 and Table 3.

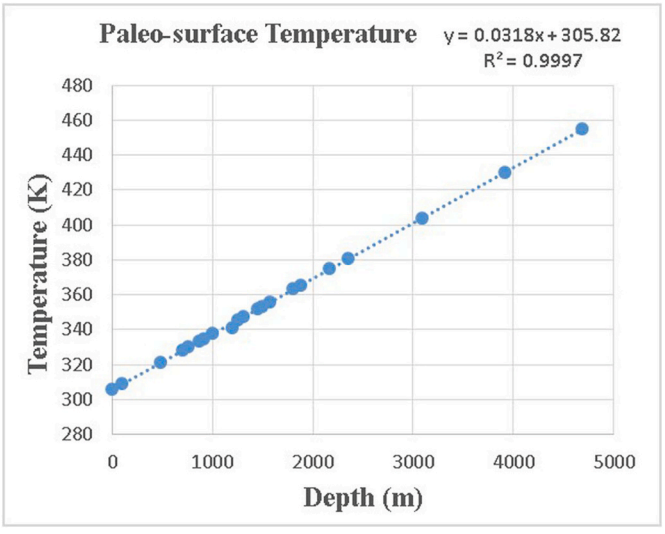

Fig. 12. Plot for paleo-surface temperature estimation from the temperature log in Well Qadirpur Deep-01.

3.7. Petroelastic analysis

Petroelastic properties for the Sembar Formation are estimated in this work from wireline-log data. To further assess the Sembar Formation, these petroelastic properties were used to evaluate its shale oil/gas potential. The compressional log (DT4P) was used to generate the p-wave velocity log (Vp). The shear log (DT4S) was used in a similar way to generate a shear-wave velocity log (Vs). Petroelastic parameters for the entire Sembar Formation encountered in Well Qadirpur Deep-01 were calculated using Vp and Vs to return properties such as B, E and PR. These are petroelastic properties that play a significant role in the identification of potential drill zones when combined with the results from TOC logs.

The ratio of uniaxial stresses to uniaxial extensional strain, under a general state of uniaxial stress, is called the Young's Modulus. It provides a measure of the degree of stiffness of a rock interval, with the relationship between E, density (ρ), Vp, and Vs being given by (Mavko and Jizba, 1990; Ali et al., 2018):

$$E = \frac{\rho Vs^2(3Vp^2 - 4Vs^2)}{Vp^2 - Vs^2} \tag{17}$$

The ratio of lateral contraction to stretching under uniaxial extension for a given homogenous isotropic rock is given by the Poisson's Ratio (PR). Low PR values correlate with the presence of gas or oil shales. The relationship between PR, Vp, and Vs is represented by the following equation (Mavko et al., 2009; Ali et al., 2018):

$$PR = \frac{0.5(Vp^2 - 2Vs^2)}{Vp^2 - Vs^2} \tag{18}$$

The parameter B of a stratigraphic unit depends on the effective stress recorded in it, the texture of the rock, strength, the lithology of the unit, and other mechanical parameters such as compressive strength to tensile strength ratio (Zhang et al., 2016). The value of B in unconventional oil and gas fields depends chiefly on rock mineralogy. Ductility is enhanced by increasing clay content and, conversely, higher brittleness relates to increasing amounts of quartz and dolomite. Rock brittleness is function of both PR and E, and is used to distinguish brittle from ductile rocks. The B can be calculated by using an empirical relation given by (Rickman et al., 2008; Ali et al., 2018):

$$B = \frac{(B_E + B_{PR})}{2} \tag{19}$$

where,

Table 3
Ages, paleo-depth and temperature history of the Sembar Formation based on data from Well Qadirpur Deep-01.

Paleo-Age	Paleo Depth	Burial Rate	Temperature history		Heating Rate (q)	TTI_{Arr}	$\sum TTI_{Arr}$	$Log_{10}\sum TTI_{Arr}$
Ma	m	m/Ma	°C	K	K/Ma			
165	0	0	33	306.15	−1.86	2.33E-07	2.33E-07	−6.63
101	776	12.12	58	331.15	0.40	1.42E-05	1.44E-05	−4.84
91	1600	82.40	84.55	357.70	2.65	1.73E-03	1.75E-03	−2.76
81	2339	73.90	108.35	381.50	2.38	8.02E-03	9.76E-03	−2.01
75	2518	29.83	114.12	387.27	0.96	5.24E-03	1.50E-02	−1.82
74	2805	287	123.37	396.52	9.25	1.25E-02	0.03	−1.56
73	2881	76	125.82	398.96	2.45	9.43E-02	0.12	−0.91
71	3111	115	137.72	410.87	5.95	0.44	0.56	−0.25
69.5	3320	139.33	149.62	422.77	7.94	0.36	0.93	−0.03
68	3120	−133.33	133.52	406.66	−10.74	0.44	1.37	0.14
61	3191	32.91	135.80	408.95	0.33	0.16	1.53	0.19
59	3237	23	137.28	410.43	0.74	0.21	1.75	0.24
58	3380	143	141.89	415.04	4.61	0.21	1.96	0.29
57	3431	51	143.53	416.68	1.64	0.21	2.18	0.34
56	3489	58	145.40	418.55	1.87	0.28	2.46	0.39
49	3688	28.42	151.81	424.96	0.92	3.91	6.37	0.80
47	3773	42.5	154.55	427.70	1.37	2.07	8.44	0.93
45	3819	23	156.03	429.18	0.74	2.69	11.13	1.05
43	3928	54.5	159.55	432.70	1.76	4.04	15.16	1.18
41	3984	28	161.35	434.50	0.90	5.64	20.80	1.31
29	4244	21.67	169.73	442.88	0.70	75.24	96.05	1.98
23.5	4504	47.27	178.10	451.25	1.52	105.23	201.28	2.30
18	4204	−54.54	168.42	441.59	−1.76	101.32	302.60	2.48
3	4497.5	19.57	177.89	451.04	0.63	264	566.59	2.75
2	4791	293.50	187.35	460.50	9.46	59.21	625.81	2.80
1	4591	−200	180.90	454.05	−6.44	72.04	697.84	2.84
0	4686	95	183.97	457.13	3.07	53.50	751.35	2.86

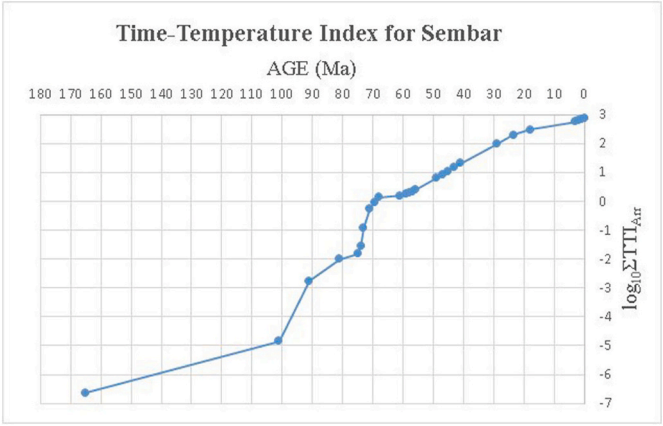

Fig. 13. Time-temperature index values for the Sembar Formation plotted against its age.

$$B_E = \frac{E - E_{min}}{E_{max} - E_{min}} \tag{20}$$

and,

$$B_{PR} = \frac{PR - PR_{min}}{PR_{max} - PR_{min}} \tag{21}$$

TThe

In Equations (19)–(21), E_{min} represents the lowest value of Young's Modulus, E_{max} is the highest value of Young's Modulus, PR_{min} is the smallest value of Poisson's Ratio and PR_{max} is the highest value of Poisson's Ratio. The petroelastic and petrophysical properties for the Sembar Formation at Well Qadirpur Deep-01 are shown in Fig. 14. Sembar Formation has a depth of 3910 m–4686 m with a thickness of 776 m, average porosity of 12.7%, effective porosity of 0.88%, and volume of shale of 77%. In order to determine the relation between the important petroelastic properties in terms of hydraulic fracturing, a cross-plot between *PR*, *E* and *B* was generated in Fig. 15.

3.8. TOC estimation from seismic data

Wireline logs are essential to estimate rock properties at relatively high resolutions. However, the problem lies in well-log data being one dimensional in nature despite its easy accessibility and low cost when compared to lab analyses and other sampling procedures such as side- and full rock coring (Schmoker, 1979, 1981). In order to tackle this problem, well-derived reservoir properties are often tied with seismic data within the known boundaries of seismic resolution using geo-statistical tools (Ali et al., 2019). Geostatistical tools used are often simple regression methods demonstrating meaningful relationships between two variables (Castagna and Backus, 1994; Leite and Vidal, 2011; Aziz et al., 2018; Ali et al., 2019). Sections thus generated for each reservoir property thus provide credible distributions for the respective property, throughout a study area, rather than being limited to a single dimension (1-D).

3.9. Acoustic impedance (AI)

TOC obtained from one dimensional well can be estimated for a larger area using seismic data by relating the *TOC* with acoustic impedance (*AI*) via a geostatistical tool. In order to do so, *AI* sections must first be compiled as discrete seismic profiles containing the stacked amplitudes obtained from the convolution of a reflectivity series with source-generated wavelets (Sheriff, 1984).

Multiple inversion techniques are available to obtain *AI* for specific seismic profiles. This study made use of relative values from Simulated Annealing Inversion (*SAI*) to generate *AI* sections. Geostatistical correlations of relative acoustic impedance and *TOC* for multiple wells have been previously applied to the Badin area in order to estimate *TOC* sections for Sembar Formation (Aziz et al., 2018).

3.10. Simulated Annealing Inversion (SAI)

Simulated Annealing Inversion (*SAI*) is an inversion technique that is

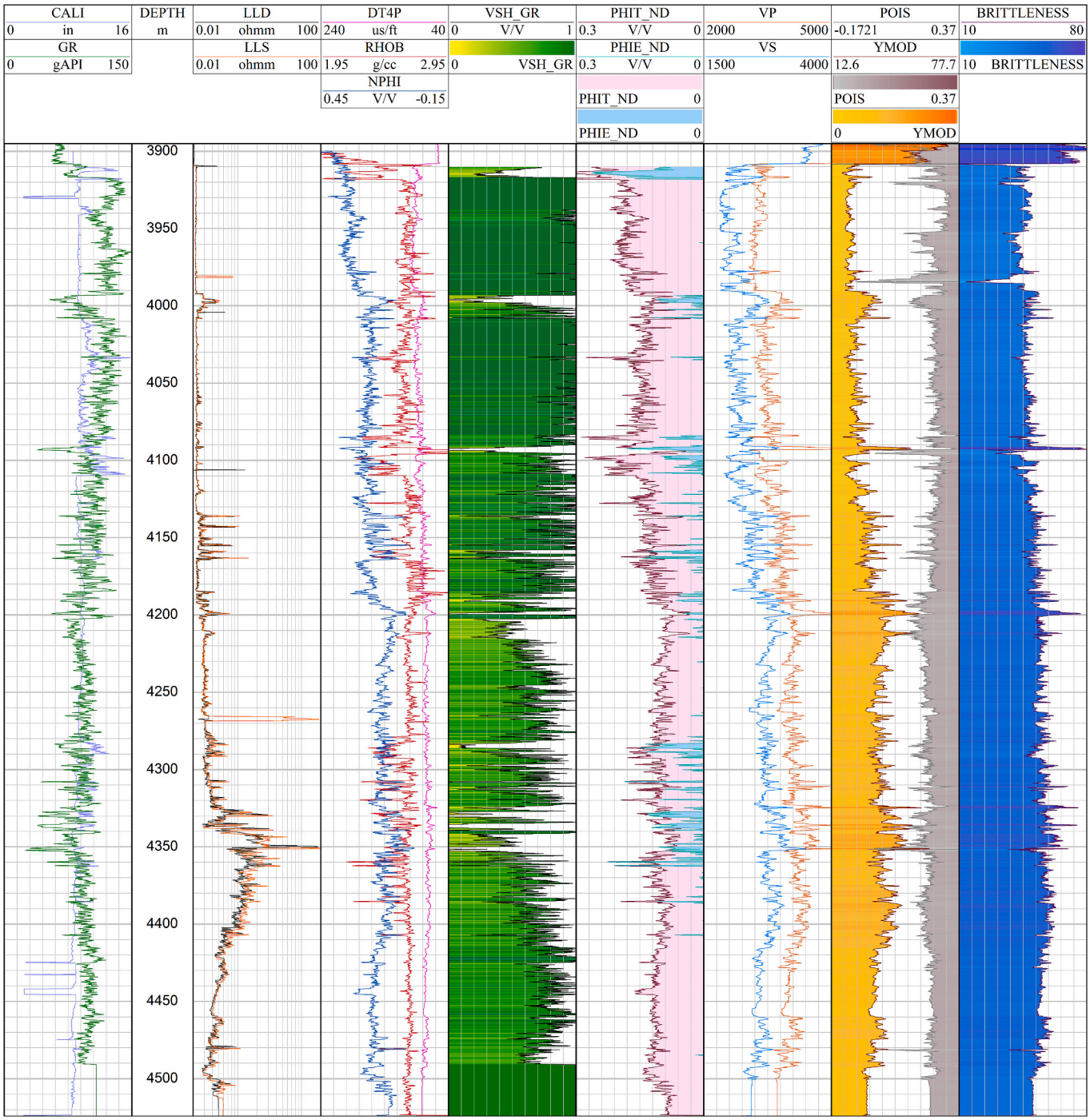

Fig. 14. Petrophysical and petroelastic properties of the Sembar Formation for Well Qadirpur Deep-01.

model-driven, being used to extract absolute and relative *AI* values of a high resolution. The inversion calculates both absolute as well as relative values of *AI*. The relative acoustic impedance (*RSAI*) extracted using this inversion technique is best used for interpreting boundaries for specific intervals. The result for *RSAI* applied to the SO-90-QPR-05 seismic section is shown in Fig. 16.

3.11. TOC analysis based on seismic data

TOC logs calculated using different techniques are calibrated with the relative AI sections previously mentioned. Bearing in mind resolution differences in both data sets, the regression technique is valid only after the well data values are upscaled in accordance with the seismic resolution (Ali et al., 2019). The vertical resolution of seismic data can be determined after extracting the dominant frequency (f) and velocity (v) at the respective zone of interest. Wavelength for the seismic data at that zone can be determined using equation (22):

$$\lambda = \frac{v}{f} \tag{22}$$

where, λ is wavelength, v is velocity (taken from the time-depth chart) and f is dominant frequency which is 25.093 Hz. In the study area, the vertical resolution of seismic data is obtained by 1/4th of the dominant wavelength (λ). The dominant frequency for seismic data is determined with the help of amplitude spectrum (Ali et al., 2019), as shown in

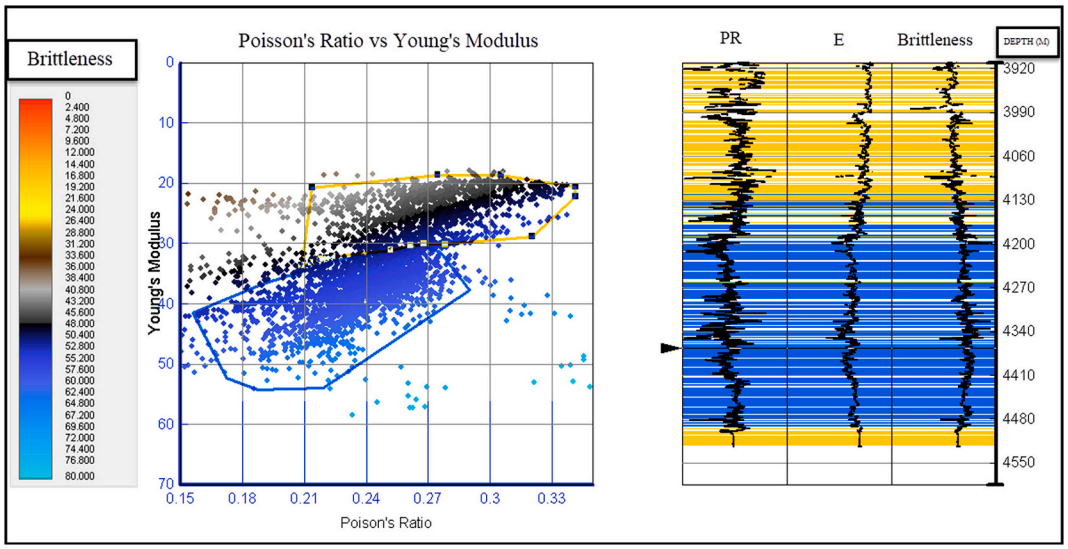

Fig. 15. Cross-plot between *PR*, *E* and *B* for locating favourable zones for hydraulic fracturing.

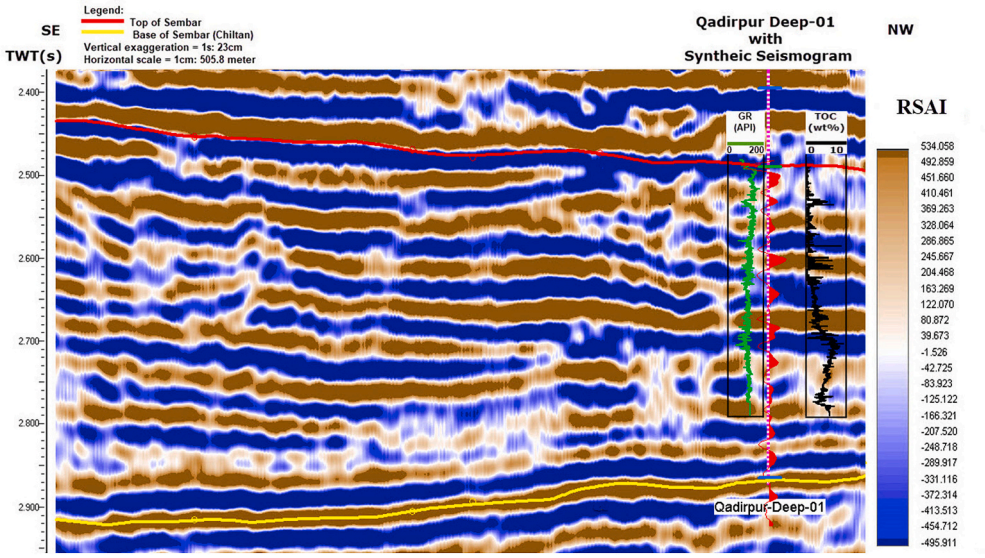

Fig. 16. *RSAI* section developed using the SAI technique for SO-90-QPR-05 seismic line.

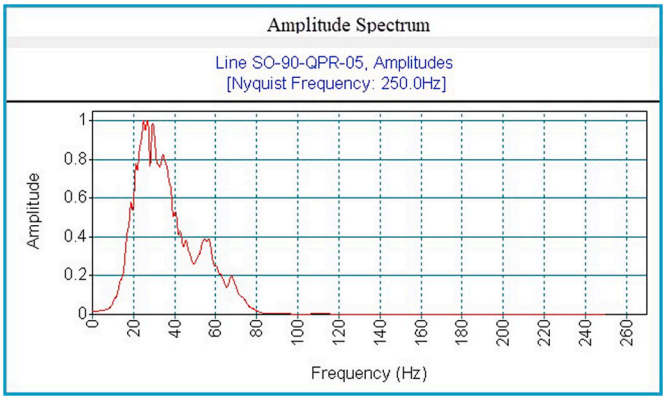

Fig. 17. Amplitude spectrum of seismic line SO-90-QPR-05. Dominant frequency is 25.093 Hz.

Fig. 17. The seismic resolution calculated at Sembar Formation comes out to be 26 m. The average (upscaled) well log value for every 26 m is further used to develop a geostatistical relation within the range of seismic resolution (Ali et al., 2019).

Values taken from *RSAI* are obtained according to the depths of upscaled well-log data. The values are then plotted against each other, with *RSAI* values on x axis and upscaled *TOC* values obtained using different methods on y axis (Figs. 18 and 19). A linear regression line is then obtained, and this should return a correlation coefficient value (R^2) above 0.7. The equation for that line is then used to develop the seismic *TOC* sections; the plots obtained for both high and low *TOC* values against the relative values of *AI* are then used to estimate the high and low *TOC* values on the seismic section (Ali et al., 2019).

3.12. Seismic TOC sections derived from RSAI

Seismic *TOC* sections were developed by correlating the *RSAI* values with Passey's separation techniques, Schmoker's method, and Schwarzkopf's technique. The sections were developed based on correlating organic maturity obtained from multiple techniques with

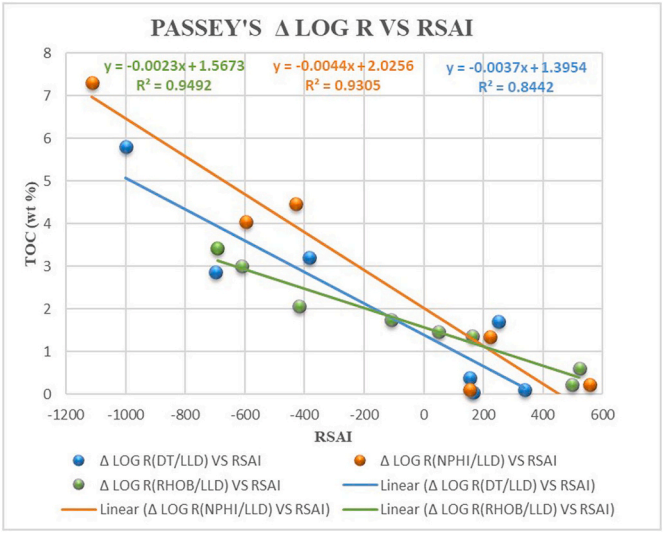

Fig. 18. Cross-plot between all three *TOC* curves generated from Passey's Δ Log R method vs. *RSAI*.

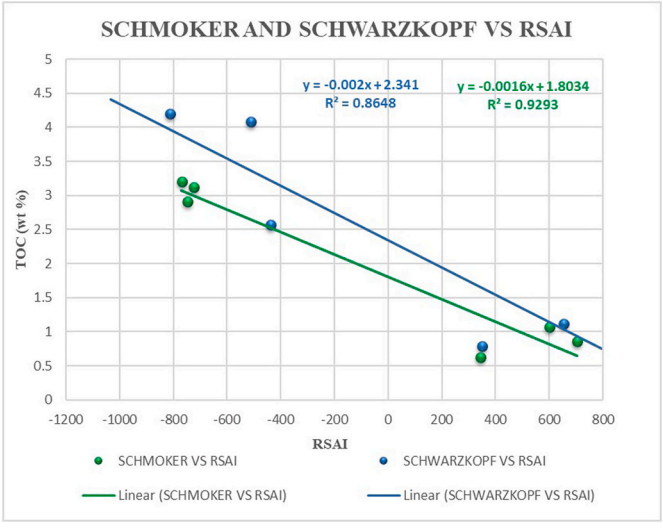

Fig. 19. Cross-plot between *TOC* estimated from Schmoker's and Schwarzkopf's technique vs. *RSAI*.

RSAI values obtained after upscaling the well-log data (Figs. A7-A11).

4. Results and discussion

4.1. Spatial distribution of the Sembar Formation

The Sembar Formation was mapped using a synthetic seismogram generated from the DT and RHOB logs of Well Qadirpur Deep–01, as a tool for seismic–to–well ties. The top of the Sembar Formation was marked at a two-way time depth of 2.47 s while the bottom was marked at 2.88 s (Fig. 5).

After carefully interpreting horizons and faults over the seismic sections, we gridded and contoured time, depth and thickness variations as shown in Figs. 6–8 respectively. Time and depth contouring reveals the presence of horst and graben structures in the study area. Time- and depth-contour maps were prepared for the Top of Sembar Formation with a contour interval of 0.004 s and 10 m, respectively. The isopach map of the formation was compiled with a contour interval of 16 m, and shows the thickness varying between 640 and 910 m (Fig. 8).

4.2. TOC estimates from well logs

Calculations of *TOC* using wireline logs from Well Qadirpur Deep–01 have been briefly described in the section "*TOC* estimation" (Figs. A1-A5). A decreasing trend in RHOB with increase in GR, DT, LLD, and NPHI values suggests the presence of a *TOC* rich interval (Passey et al., 1990; 2010; Aziz et al., 2018). Estimated *TOC* values for the Sembar Formation vary between 2 and 4 wt% (Table 4).

4.3. Thermal maturity modelling

The burial history of the study area records a relatively low subsidence rate of 12.13 m/Ma from 165 Ma to 101 Ma (Fig. A6). The basin records a phase of relatively rapid subsidence from 101 Ma until 69.5 Ma (100.4 m/Ma on average) after which it was uplifted. Three episodes of tectonic uplift occurred over the history of the basin, during late Cretaceous (69.5 Ma to 68 Ma) with an average uplift of 133 m/Ma, early Miocene (23.5 Ma to 18 Ma) with an average uplift rate of 54 m/Ma, and Pleistocene (2 Ma to 1 Ma) with an average uplift of 200 m/Ma (Fig. A6). Tectonic uplift has had a clear impact on source-rock maturity; however, the prolonged burial intervals, consistent overburden pressure and large maximum depth of up to 4686 m recorded in the study area have provided a suitable environment for the development of hydrocarbons (Table 3).

The temperature history of the Sembar Formation has been reconstructed in this work using temperature data for Well Qadirpur deep-01, as shown in Fig. 11. The paleo-temperature curve for the Sembar Formation reveals a gradual increasing trend from 165 Ma to 101 Ma, followed by a sharp increase in temperature from 101 Ma to 69.5 Ma (Fig. 11). The paleo-surface temperature estimated from the log is 306.15 K (Fig. 12). In more detail, the Sembar Formation reached a temperature of about 413.05 K (Table 3) followed by a decrease of 279.55 K in the formation during the first uplift episode. Afterwards, regional subsidence caused an increase in temperature until the second uplift episode, which caused a decrease of 282.75 K. The third episode of tectonic uplift caused a decrease of 279.55 K. The Sembar Formation thus records a temperature of 456.15 K at present (Table 3).

The thermal maturity of organic matter was calculated in a third step in our analysis using the Arrhenius equation. The scales of the time-dependent temperature index (TTI_{Arr}) developed using the Arrhenius equation, and its respective *Ro* values, vary from a $log_{10}\Sigma TTI_{Arr}$ value of −4 for *Ro* 0.5% to a $log_{10}\Sigma TTI_{Arr}$ value of +3 for *Ro* 2% (Wood, 2017).

The low values $log_{10}\Sigma TTI_{Arr}$ for the Sembar Formation from 165 Ma to 91 Ma show that the formation was immature during this period, at a time when the unit was subjected to ~343.15 K (Fig. 13). Temperature and pressure leading to the generation of hydrocarbons started after 91 Ma. When the Sembar Formation recorded its first uplift episode, hydrocarbon generation was ongoing and responding to temperatures as high as 412.15 K, correlating to a burial depth of 3320 m and a $log_{10}\Sigma TTI_{Arr}$ value of −0.032 (Table 3). In spite of a reduction in hydrocarbon generation caused by tectonic uplift (Fig. A6), the $log_{10}\Sigma TTI_{Arr}$ values reaching up to 2.87 at a burial depth of 4686 m, and the temperature values of up to 456.15 K, confirm hydrocarbons are being generated at present (Fig. 13).

Table 4
Average *TOC* values estimated using the Passey's, Schmoker's and Schwarzkopf's methods.

QADIRPUR DEEP – 01					
LOM	PASSEY'S Δ Log R METHOD			SCHMOKER'S METHOD	SCHWARZKOPF'S METHOD
	DT/LLD	RHOB/LLD	NPHI/LLD		
	WEIGHT PERCENTAGE (wt%)				
7	2.54	3.85	3.53	2.03	3.57

4.4. Petrophysical and petroelastic properties

Conventional petrophysical properties for the Sembar Formation are shown in Fig. 14. The petroelastic properties are important to study whether the formation is prone to hydraulic fracturing, which is an essential requisite for unconventional oil and gas fields. The parameter *B* was calculated in Fig. 14 to investigate the feasibility of hydraulic fracturing in the study area – it reveals a potential oil/gas zone in the lower portion of the Sembar Formation. Total porosity values are low (12.7%), indicating that the degree of compaction recorded by shales in this formation is high. The cross-plot in Fig. 15 proves that the lower part of the Sembar Formation has a relatively low *PR*, relatively high values of *E*, and relatively high brittleness.

Generally, the ductility of shales increases with increasing organic content (Verma et al., 2018). Yet, a high degree of compaction, together with the mineralogy of the source rock, generate perfect conditions for hydraulic fracking in probable hydrocarbon zones (Verma et al., 2018). A good unconventional source rock is one with good to excellent *TOC* values and yet has a mineralogy which makes it brittle. Furthermore, it should also be noted that *TOC* should not be higher than a certain threshold value, as in this case rock will tend to overmature under certain conditions, making it not feasible for hydrocarbon exploitation. Thus, 2–4 wt% *TOC* values (Table 4), along with 60–80% *B* values (Figs. 14 and 15) make the Sembar Formation suitable for hydraulic fracking.

4.5. Seismic-based spatial TOC estimation

In order to display *TOC* values throughout the Sembar Formation, rather than in 1-D along a single well, a linear equation between *RSAI* section (Fig. 16) and upscaled *TOC* values on the basis of dominant frequency and seismic resolution (Fig. 17) should be developed.

The *TOC* and *RSAI* curves have been plotted for both high and low *TOC* values and their respective *RSAI* values (Figs. 18 and 19). The trend between the two variables is inverse for both cases, with correlation coefficients of $R^2 = 0.8442$ (Passey's (DT/LLD)), $R^2 = 0.9305$ (Passey's (DT/LLD)), $R^2 = 0.9492$ (Passey's (DT/LLD)), $R^2 = 0.9293$ (Schmoker), and $R^2 = 0.8648$ (Schwarzkopf). The best fit regression line equations are given as:

$$TOC\ DT/LLD = -0.0037\ RSAI + 1.3954 \quad (23)$$

$$TOC\ NPHI/LLD = -0.0044\ RSAI + 2.0256 \quad (24)$$

$$TOC\ RHOB/LLD = -0.0023\ RSAI + 1.5673 \quad (24)$$

$$TOC\ SCHMOKER = -0.0016\ RSAI + 1.8034 \quad (21)$$

$$TOC\ SCHWARZKOPF = -0.002\ RSAI + 2.341 \quad (22)$$

The sections shown in Figs. A7 to A11 reveal variable *TOC* trends. The *TOC* values vary from 2 to 4 wt%, confirming the Sembar formation to be a shale-gas unconventional source. The upper part of the Sembar Formation shows promising *TOC* values. The central portion of the formation has a varying *TOC* values with patches of up to 4 wt% (Figs. A7-A11). The lower part of Sembar Formation turns out to be the best locality for hydraulic fracturing as results show high *TOC* values in this interval. A similar trend can be detected in the sections developed using various methodologies, confirming the validity of our results.

4.6. Comparison of multiple case studies

In order to justify and validate the results found in this research, the results have been compared with multiple case studies carried out in various localities for *TOC* estimation in Sembar Formation (Table 5). The comparison shows that the results from our analysis are in alignment with the previous studies which also includes core sample analysis (Table 5). According to Sohail et al. (2020), the average *TOC* value of the Sembar Formation is 3 wt% based on core data samples and log analysis of Well Y in the Lower Indus Basin (Table 5). Similarly, Robison et al. (1999) has evaluated the *TOC* values for the Sembar Formation in Well Sann-1, located in Petaro area, Lower Indus Basin (Table 5). According to Ahmad et al. (2012), *TOC* values found in the Punjab Platform, Sulaiman Foldbelt, Lower Indus Platform, and Kirthar Foldbelt are <0.5–1.64 wt%, 0.56–4.33 wt%, <0.5–4.15 wt%, and 0.83–3 wt% respectively.

4.7. Implications of the study

The *TOC* ranges estimated for the Sembar Formation lie between 2 and 4 wt%, qualifying it as a good to excellent source rock (Peter et al., 1986; Aziz et al., 2018). Samples of the Sembar Formation were investigated in the laboratory for *TOC* content by Wandrey et al. (2004) to show a range from 0.5 to 3.5 wt%. The results from our study are therefore verified by these laboratory values. Furthermore, studies show Types II and III kerogen are present in the Sembar Formation (Wandrey et al., 2004; Ahmad et al., 2011; Sheikh and Giao, 2017; Aziz et al., 2018), with *TOC* values up to 9.5 wt% found in core samples. Petroleum system modelling (PSM) applied to the Sembar Formation shows that prolific shales lie in the temperature window suitable for gas and oil generation (Sheikh and Giao, 2017).

Due to the unavailability of multiple wells and 3D seismic data in the study area, *TOC* values could not be determined for regional grids. However, the strike line SO-90-QPR-05, which is NW–SE oriented, has been used in our analysis. This study shows high *TOC* values within the Sembar Formation, confirming the maturity of kerogen within this same formation, and presents it as a good potential unconventional resource. The paleo-geographic location of the Sembar Formation at the time of deposition played a key role in contributing to these high *TOC* values. The environment and the age of deposition suggests a northward drift of the Indian plate during the late Jurassic and Lower Cretaceous, leading this tectonic plate into increasingly warmer climates (Scotese et al., 1988; Aziz et al., 2018). By the Lower Cretaceous, marine shales in the Sembar Formation accumulated over Jurassic Chiltan limestone on the paleo-continental shelves of the Indian plate, at a Latitude of 20°S and Longitude of 68°E (Scotese et al., 1988; Aziz et al., 2018). High organic

Table 5
Comparison of average *TOC* values estimated for the Sembar Formation at different localities of the Lower Indus Basin, Pakistan.

Case Study	Sohail et al. (2020)	Robison et al. (1999)	Aziz et al. (2018)			(Current Study)
Formation	Sembar	Sembar	Sembar			Sembar
Locality	Lower Indus Basin	Petaro	Badin			Qadirpur
Well	Y	Sann-1	A	B	C	Qadirpur Deep-01
Depth (m)	4046–4071	3455–3584	2400–2840	2400–2840	2510–2800	3910–4686
Average TOC-wt% (Core)	3	3.73375	–	–	–	–
Average TOC-wt% (Passey (DT/LLD))	3	–	2.5	2.2	4	2.54
Average TOC-wt% (Passey (RHOB/LLD))	–	–	–	–	–	3.85
Average TOC-wt% (Passey (NPHI/LLD))	–	–	–	–	–	3.53
Average TOC-wt% (Schwarzkopf)	–	–	3.7	2.2	2.3	3.57
Average TOC-wt% (Schmoker)	–	–	–	–	–	2.03

production rates led to enhanced *TOC* concentration owing to the suitable paleo-environment at the time of deposition. Slow decomposition and high production rates for the organic matter subsequently led to favourable organic matter preservation, as shown by the thermal maturity modelling for the Sembar Formation in Fig. A6 and Figs. 11–13.

Rock brittleness is a parameter indicating how easily a rock can fail (Obert and Duvall, 1967; Zhang et al., 2016; Kang et al., 2020). Fractures play an essential role in terms of hydrocarbon production as it makes extraction feasible, but unconventional resources lack such a characteristic feature and often require fractures to be stimulated in a volume of rock. As high *B*, low *PR*, and high *E* are typical of more fragile rocks (Rickman et al., 2008), the petroelastic properties in this work delineate the probable zones that are prone to hydraulic fracturing in the Sembar Formation (Fig. 15).

The Lower and Central Indus Basin have been evaluated to typically reveal an economic depth for shale gas at about 3500 m, contrasting with the 1000–3000 m that is typical for unstable tectonic fold-and-thrust belts (Ahmad et al., 2011). According to our data, the Sembar Formation in the Qadirpur area has an economical depth starting at about 3600 m below the surface (Fig. 7), with significant thickness (Fig. 8) and good to excellent *TOC* values (Table 4).

The Sembar Formation also occurs to the east of the study area towards the Rajasthan Basin, in the Indian subcontinent, as well as to the west into the Zagros fold-and-thrust belt in Iran (Klett et al., 2011; Opera et al., 2013; Aziz et al., 2018). This unit comprises the most productive shale gas reserves in their respective basins (Klett et al., 2011; Opera et al., 2013; Aziz et al., 2018). While the Gurpi and Kazdumi formations of the Zagros fold-and-thrust belt have *TOC* values between 1.7 to 2.4 wt % and 1.5 to 3.92 wt% respectively (Opera et al., 2013; Aziz et al., 2018), the Ghaggar-Harka formation of the Rajasthan Basin has not been studied due to lack of available well data (Farrimond et al., 2015; Aziz et al., 2018). The methodology followed in this study might be of help for unconventional resource exploration in such under-explored basins around the globe.

The results presented in this study, however, are still limited to two dimensions. A similar methodology can be carried out in the future to a 3D seismic cube for generating the *RSAI* grid rather than a section. This grid can be correlated in geostatistical terms to the *TOC* values using at least three or more wells to obtain an accurate *TOC* seismic grid. This grid would be three dimensional and therefore provide further access to Sembar Formation's characterisation as a source rock. Furthermore, the results from the calculated *TOC* logs can be correlated with core data, if available, from the respective wells to confirm the results.

5. Conclusions

The analysis of the Sembar Formation within Qadirpur area of Central Indus Basin, undertaken in this work, returned a series of parameters that allowed a better characterisation of its economic potential as an unconventional resource. In summary, the main results of this work are as follows:

a) The Sembar Formation is an ideal shale gas unconventional resource based on the geochemical properties of its organic matter, its depositional setting, thermal maturity, thickness, petrophysical and petroelastic properties.
b) Multiple techniques for *TOC* evaluation applied to wireline data from Well Qadirpur Deep–01 revealed high (2–4 wt%) *TOC* values in the Sembar Formation. Seismic based *TOC* estimations for reservoir scale were undertaken by correlating the *RSAI* section of the SO-90-QPR-05 seismic line with the upscaled *TOC* logs using good correlation coefficient values.
c) Data acquired from each analytical method show high *TOC* values throughout the Sembar Formation along the SO-90-QPR-05 seismic line.
d) Thermal maturity modelling, including burial history, paleo-depth development, paleo-temperature evaluation and estimation of time-temperature index, confirms the Sembar Formation to be mature.
e) The presence of low *PR*, relatively high E, and high *B* values particularly for lower portion of the Sembar Formation deems it excellent for hydraulic fracturing.
f) Along with high *TOC* and high brittleness values, a thickness range of 640–910 m and a sub-surface depth starting at 3600 m makes the Sembar Formation a good to excellent unit to exploit as an unconventional resource.

The methodology used in this study will likely promote the further investigation of the Sembar Formation as an unconventional resource. It can also be considered as applicable approach to the analysis and identification of potential shale-gas plays in other parts of South Asia, and the world.

Authors agreement

Dr. Aamir Ali put forward the idea and helped with the provision of methodology for this research as well as assessed the results of the study. Mr. Yawar Amin, an MS student of Dr. Aamir Ali, implemented the methodology and carried out the research. Dr. Tiago M. Alves gave technical support and contributed in finalising the manuscript. The statement that all authors have approved the final article should be true and included in the disclosure. All authors have approved the final article should be true and included in the disclosure.

Declaration of competing interest

The authors declare that they have no known competing financial interests or personal relationships that could have appeared to influence the work reported in this paper.

Acknowledgements

The authors would like to thank Directorate General of Petroleum Concessions (DGPC), Pakistan, for allowing the use of seismic and well-log data for research and publication purposes and Department of Earth Sciences, Quaid-i-Azam University, Islamabad, Pakistan, Cardiff University, UK for providing the basic requirements to complete this work. We would like to thank IHS and CGG GeoSoftware for providing the software licenses (Kingdom and Powerlog respectively) without which this work would not have been possible. We also acknowledge the constructive comments of Executive Editor Zhejun Pan and one anonymous reviewer, which greatly improved an earlier version of this manuscript.

List of Figures in Appendix

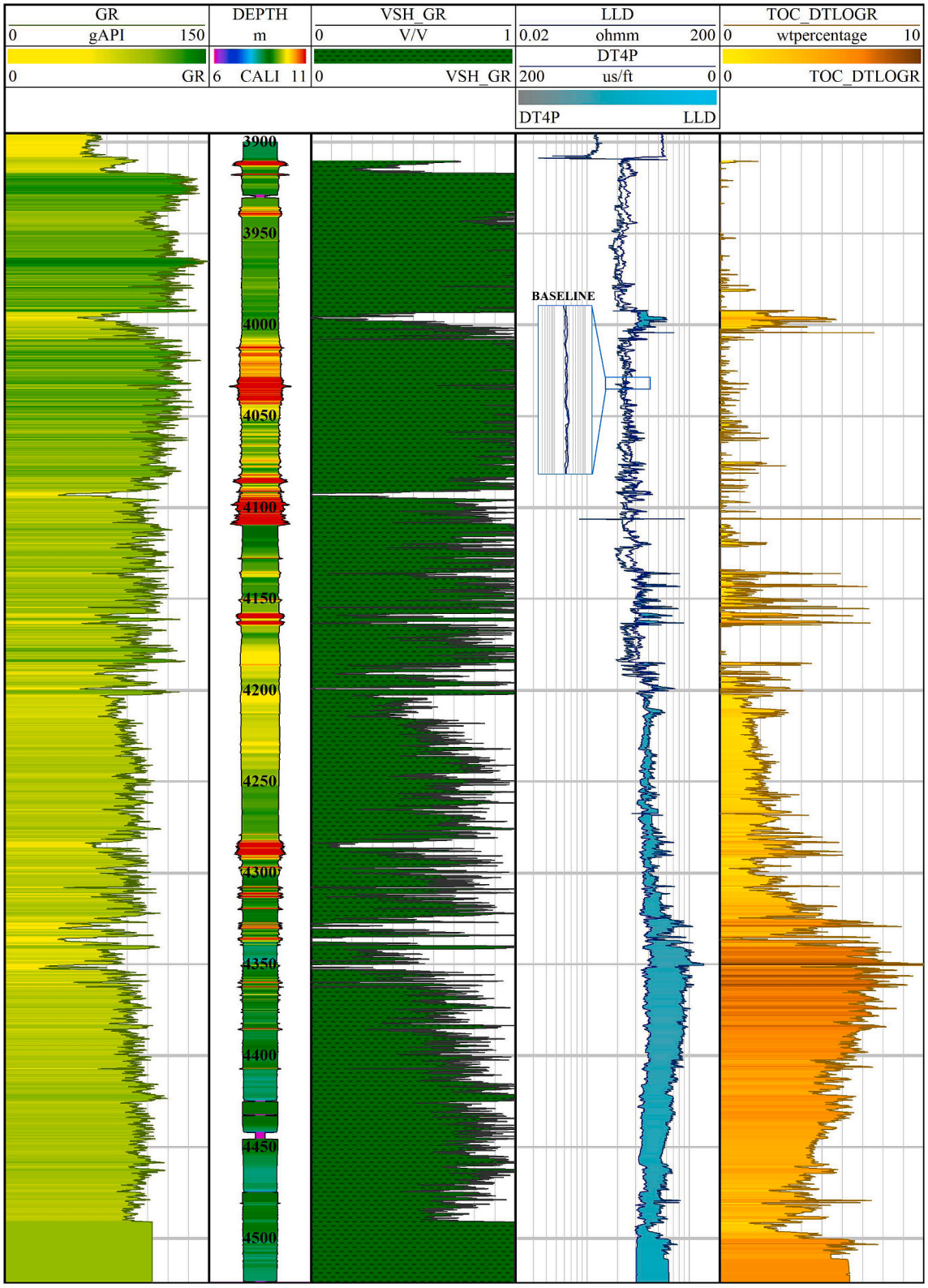

Fig. A1. DT/ LLD overlay for *TOC* estimation in the Sembar Formation, Well Qadirpur Deep – 01. The Passey's Δ Log R value for separation between DT log and LLD gives an average *TOC* value of 2.54 wt%.

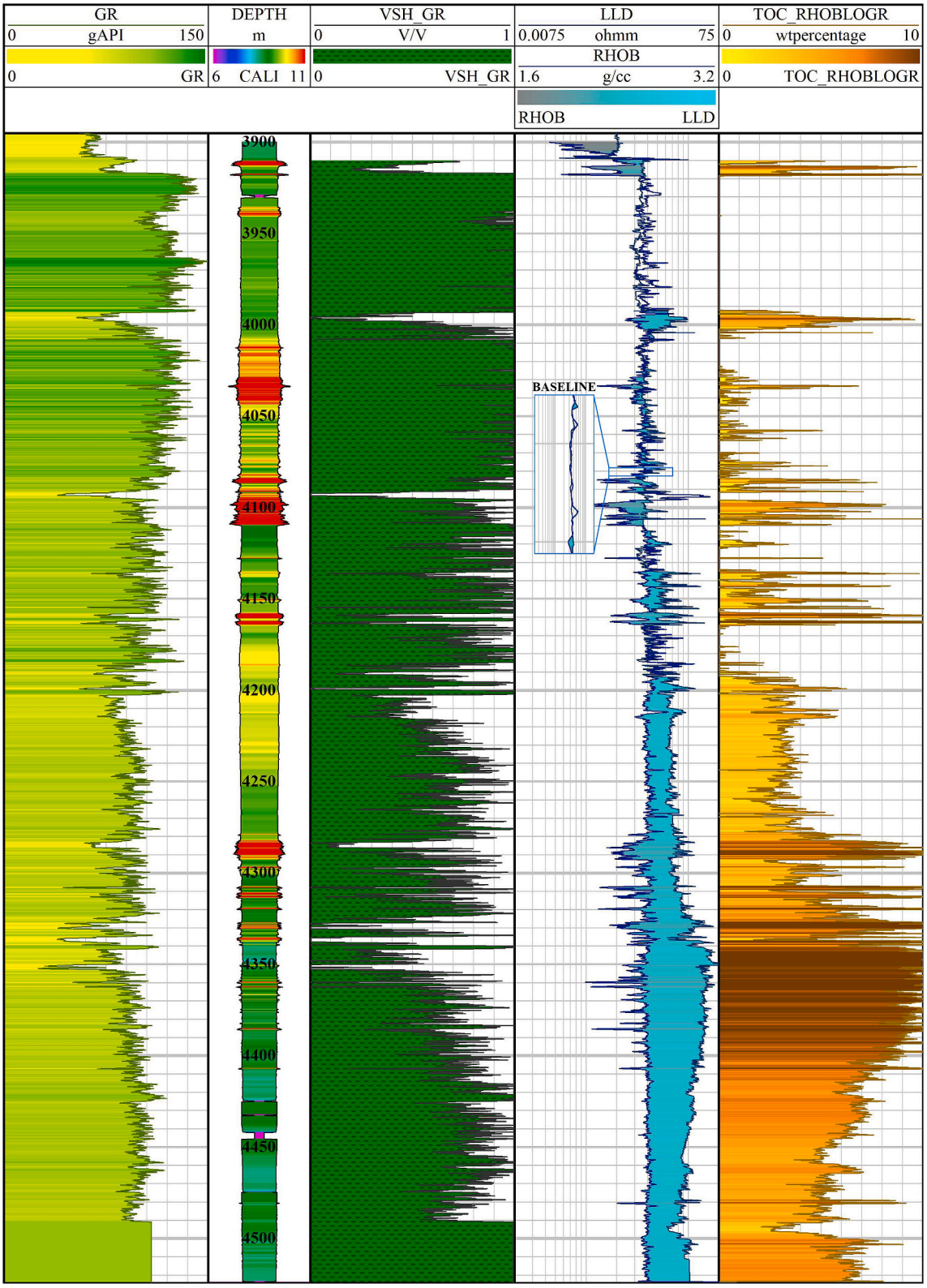

Fig. A2. *TOC* estimation via a RHOB/ LLD overlay for the Sembar Formation, Well Qadirpur Deep-01. RHOB and LLD separation produces *TOC* values when utilized in Passey's Δ Log R equation. A mean value of 3.85 wt% was estimated.

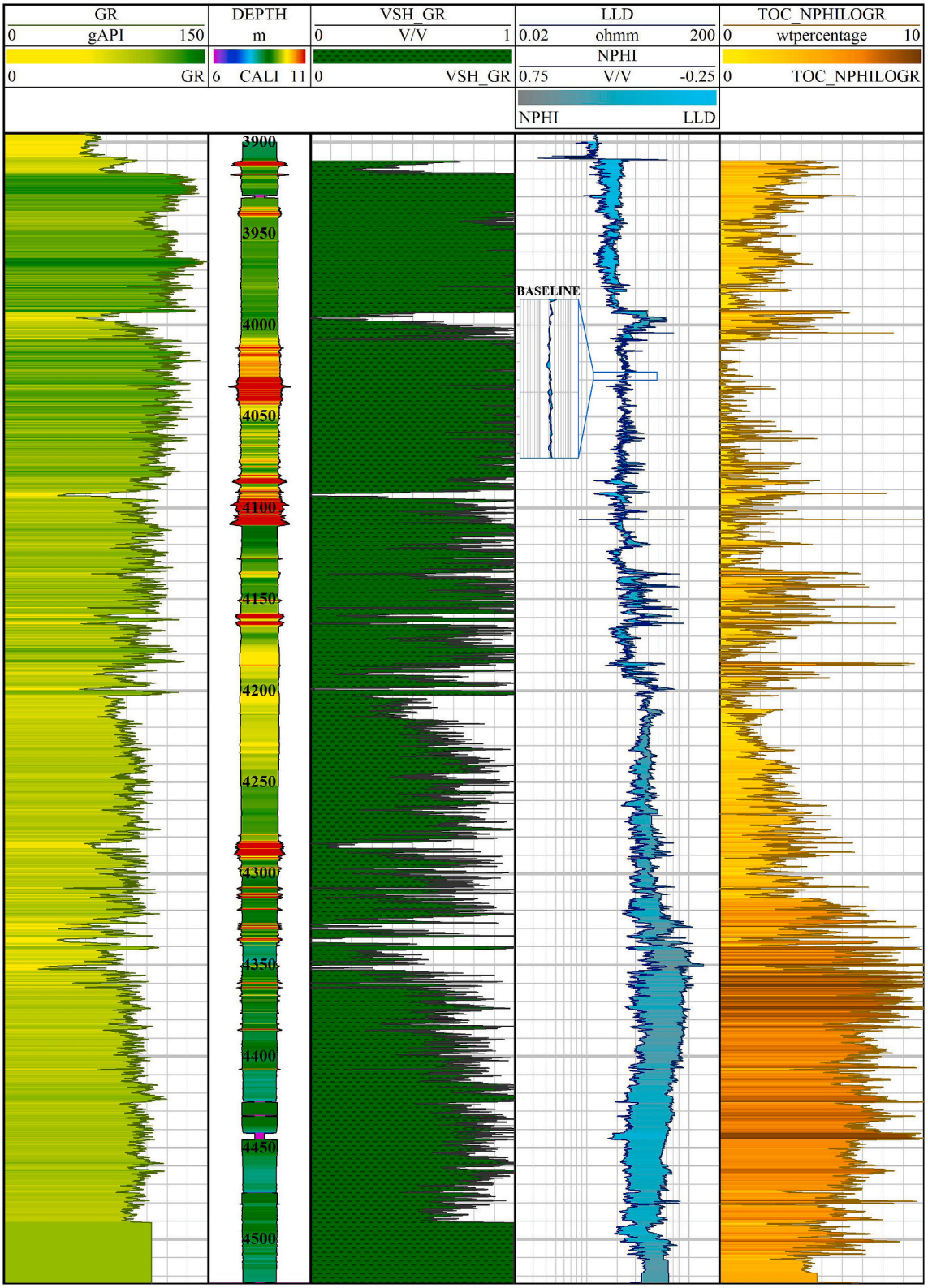

Fig. A3. *TOC* calculation for the Sembar Formation using NPHI/LLD logs for Well Qadirpur Deep – 01. The Passey's overlay technique using NPHI/LLD separation returns an average *TOC* value of 3.53 wt% for the Sembar Formation.

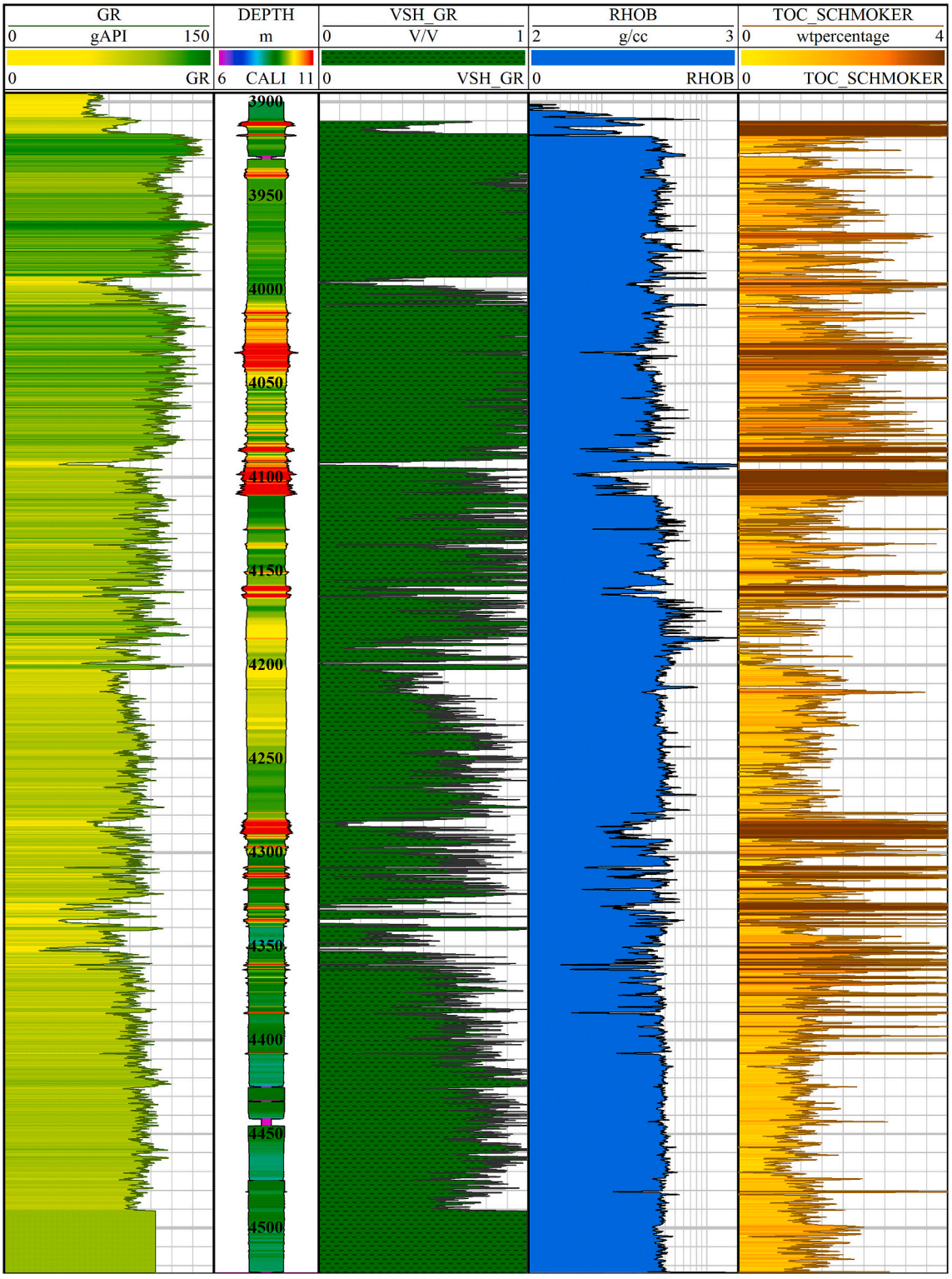

Fig. A4. Schmoker's Method for calculating *TOC* values. The Schmoker's method is entirely based on the use of RHOB values. The averaged *TOC* value obtained from the Schmoker's method is 2.03 wt%.

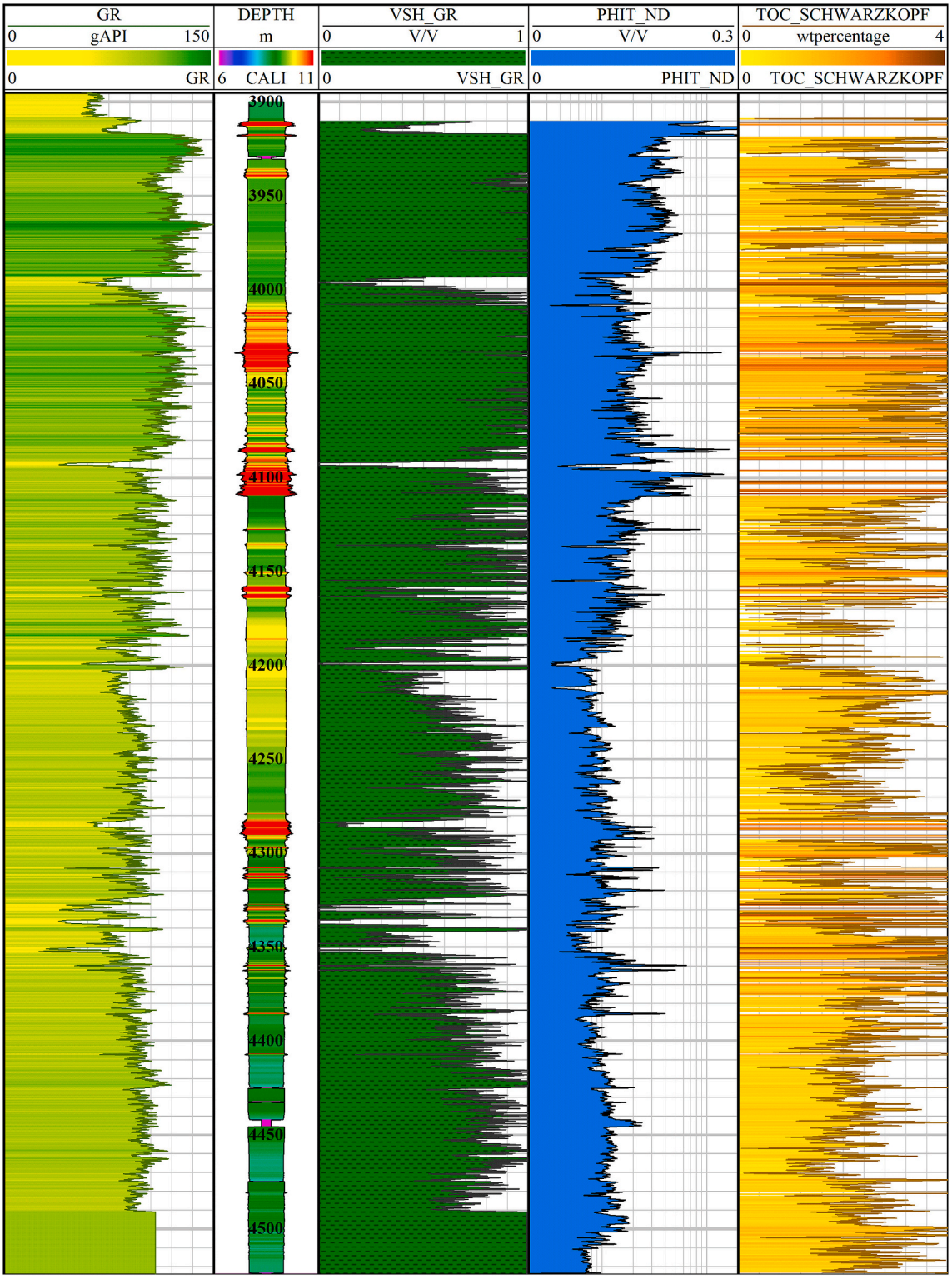

Fig. A5. Schwarzkopf's method for estimating *TOC* values. The Schwarzkopf's method estimates *TOC* on the basis of variation between source rock and non-source rock parameters. The principal wireline data used is the porosity log. The average *TOC* value for Well Qadirpur Deep – 01 approaches 3.57 wt%.

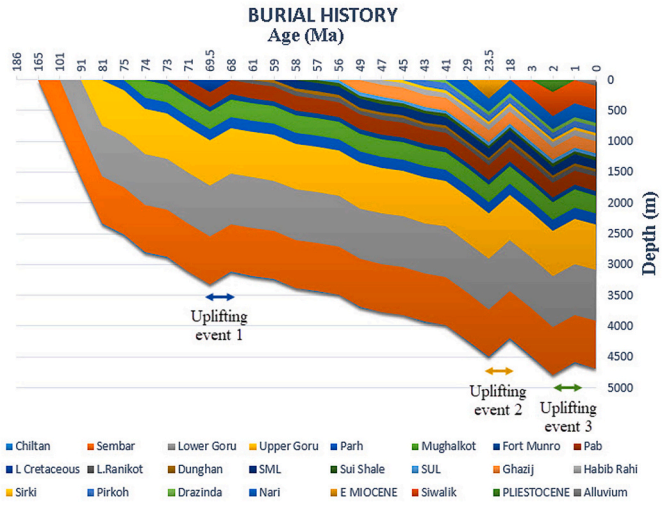

Fig. A6. Burial history of stratigraphic formations in the Qadirpur area calculated using well-log and formation-top data.

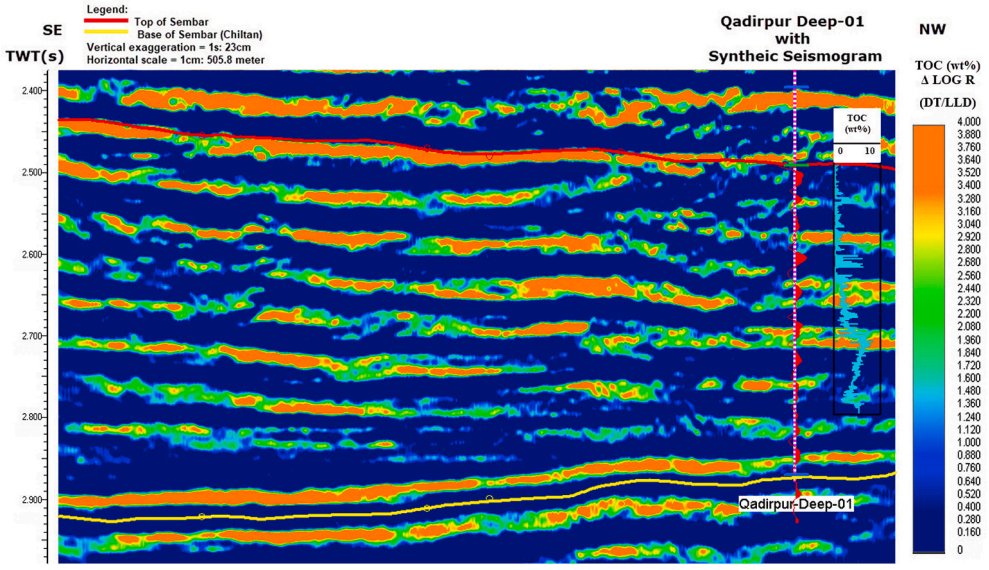

Fig. A7. *TOC* section generated using Passey's Δ Log R (DT/LLD) vs. *RSAI* cross-plot.

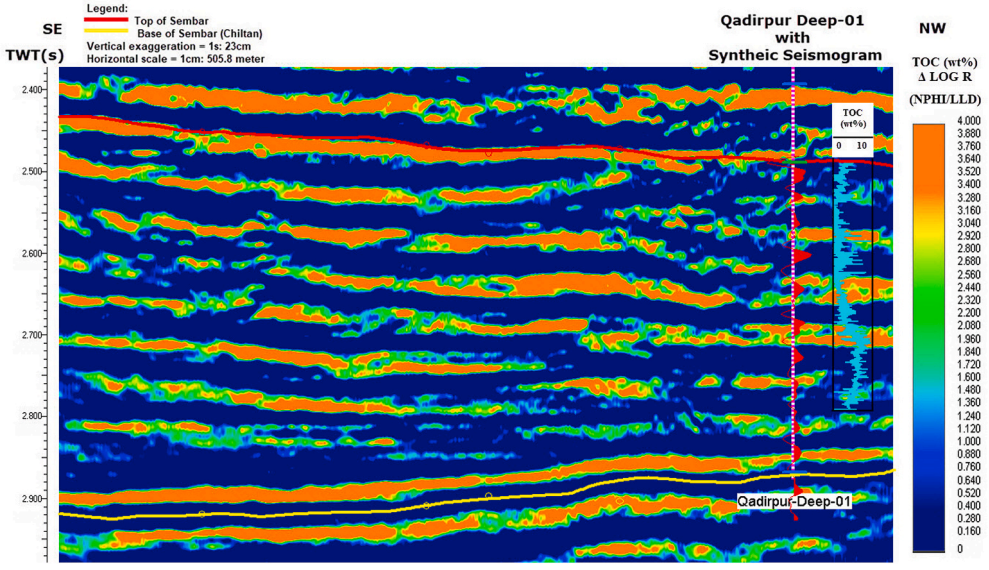

Fig. A8. *TOC* section generated using Passey's Δ Log R (NPHI/LLD) vs. *RSAI* cross-plot.

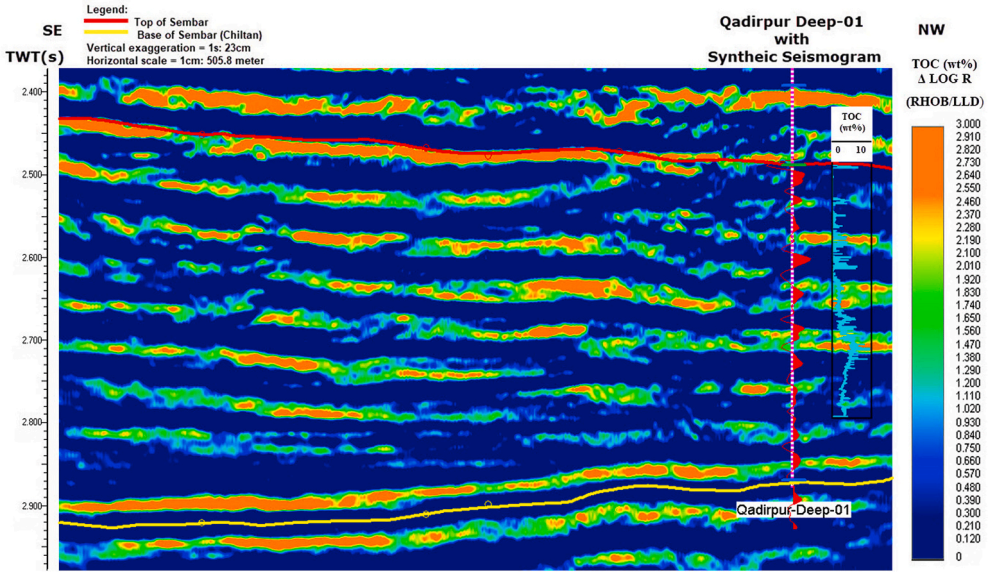

Fig. A9. *TOC* section generated using Passey's Δ Log R (RHOB/LLD) vs. *RSAI* cross-plot.

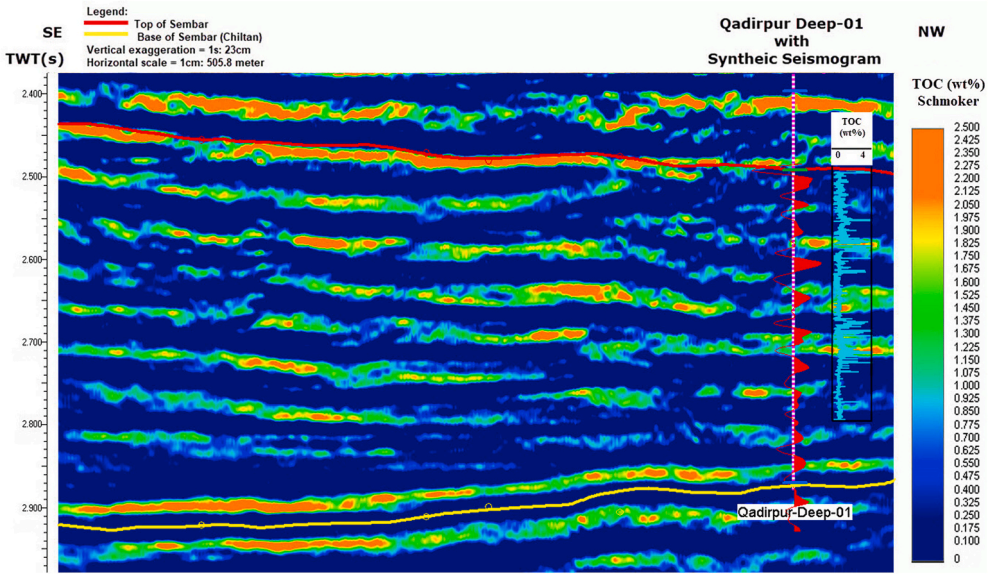

Fig. A10. *TOC* section generated using Schmoker's method vs. *RSAI* cross-plot.

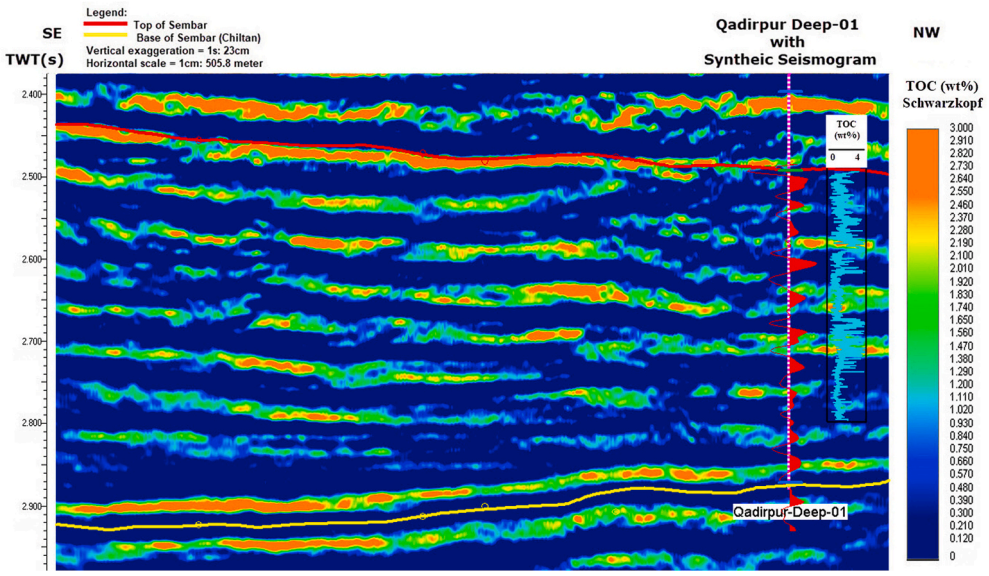

Fig. A11. *TOC* section generated using Schwarzkopf's technique vs. *RSAI* cross-plot.

References

Ahmad, N., Mateen, J., Shehzad, K., Mehmood, N., Arif, F., 2011. Shale gas potential of lower cretaceous Sembar formation in middle and lower Indus Basin, Pakistan. In: Assoc Pet Geol/Soc Pet Explor-Ann Tech Confer, pp. 235–252.

Ahmad, N., Mateen, J., Shehzad, K., Mehmood, N., Arif, F., 2012. Shale gas potential of lower cretaceous Sembar formation in middle and lower Indus sub-basins, Pakistan. In: Adapted from Oral Presentation at PAPG/SPE Annual Technical Conference 2011, Islamabad, Pakistan, November 22-23, 2011.

Ahmed, W., Azeem, A., Abid, M.F., Rasheed, A., Aziz, K., 2013. Mesozoic structural architecture of the middle Indus Basin, Pakistan—controls and implications. In: PAPG/SPE Ann. Tech. Conf, Islamabad, Pakistan, pp. 1–13.

Alam, M.S.M., Wasimuddin, M., Ahmad, S.S.M., 2002. Zaur Structure, a Complex Trap in Poor Seismic Data Area. BP Pakistan Exploration and Production Inc. PAPG/SPE ATC conference, Islamabad, Pakistan, pp. 1–3.

Ali, A., Ahmad, Z., Akhtar, G., 2005. Structural interpretation of seismic profiles integrated with reservoir characteristics of Qadirpur area. Pak. J. Hydrocarb. Res. 15, 25–34.

Ali, A., Alvesb, T.M., Saada, F.A., Ullah, M., Toqeer, M., Hussain, M., 2018. Resource potential of gas reservoirs in South Pakistan and adjacent Indian subcontinent revealed by post – stack inversion techniques. J. Nat. Gas Sci. Eng. 49 (2018), 41–55.

Ali, A., Ullah, M., Hussain, M., Bhatti, A.S., Khaista, R., 2017. Estimation of shale oil/gas potential of a Paleocene-eocene succession. A case study from the Meyal area, Potwar basin, Pakistan. Acta Geol. Sinica Eng. Ed. 9 (6), 2180–2199.

Ali, A., Younas, M., Ullah, M., Hussain, M., Toqeer, M., Bhatti, A.S., Khan, A., 2019. Characterization of secondary reservoir potential via seismic inversion and attribute analysis: a case study. J. Petrol. Sci. Eng. 178, 272–293.

Alyousuf, T., Algharbi, W., Algeer, R., et al., 2011. Source Rock Characterization of the Hanifa and Tuwaiq Mountain Formations in the Arabian Basin Based on Rock-Eval Pyrolysis and the Modified Delta Log R Method. SPE/DGS Saudi Arabia Section Technical Symposium and Exhibition.

Asim, S., Qureshi, S.N., Asif, S.K., Abbasi, S.A., Solangi, S., Mirza, M.Q., 2014. Structural and stratigraphic correlation of seismic profiles between drigri anticline and Bahawalpur high in central Indus Basin of Pakistan. Interpret. J. Geosci. 2014 (5), 1231–1240.

Aziz, O., Hussain, T., Ullah, M., Bhatti, A.S., Ali, A., 2018. Seismic based characterization of total organic content from the marine Sembar shale, Lower Indus Basin, Pakistan. Mar. Geophys. Res. 1–18.

Blackwell, D.D., Richards, M., 2004. Calibration of the AAPG geothermal survey of North America BHT data base. In: AAPG Annual Meeting, Dallas, Tx, Paper, 87616: 2004.

Bucker, C., Rybach, L., 1996. A simple method to determine heat production from gamma-ray logs. Mar. Petrol. Geol. 13 (4), 373–375.

Castagna, J.P., Backus, M.M., 1994. Offset dependent reflectivity: theory and practice of AVO analysis. Investigat. Geophys. 8, 317–332.

Connan, I., 1974. Time-temperature Relation in Oil Genesis: AAPG Bulletin, vol. 58, pp. 2516–2521.

EIA, U., 2013. Annual Energy Outlook. US Energy Information Administration, Washington, DC, pp. 60–62.

Eickhoff, G., Alam, S., 1991. On the Petroleum Geology and Prospectivity of Kirther Range and Sibi Trough, Southern Indus Basin. BGR/HDIP, Hannover, Pakistan.

Eshkalak, M.O., Mohaghegh, S.D., Esmaili, S., 2014. Geomechanical properties on unconventional shale reservoirs. J. Petrol. Eng. 2014, 961641.

Farrimond, P., Naidu, S.B., Burley, S.D., Dolson, J., Whiteley, N., Kothari, V., 2015. Geochemical characterization of oils and their source rocks in the Barmer Basin, Rajasthan, India. Pet Geo. Soc. 21, 301–321.

Galasso, F., Fernandes, P., Montesi, G., Marques, J., Spina, A., Pereira, Z., 2019. Thermal history and basin evolution of the Moatize - minjova Coal Basin (N'Condédzi sub-basin, Mozambique) constrained by organic maturation levels. J. Afr. Earth Sci. 153, 219–238.

Gao, Y., Wen, Z., Xu, Y., Song, H., Li, W., Yu, Y., Ke, C., 2020. Geochemical characteristics of the Chang 7 organic-rich fine-grained sedimentary rocks and its relationship with the tight oil in Longdong area, Northwest China. J. Petrol. Explor. Prod. Technol. 10, 1803–1816.

Glorioso, C.J., 2012. Unconventional reservoirs: basic petrophysical concepts of shale gas. SPE 153004.

Habicht, J.K.A., 1964. Comment on the history of migration in the gifhorn trough. In: Proceedings of the Sixth World Petroleum Congress, Section 1, p. 480.

Hill, R.J., Zhang, E., Katz, B.J., et al., 2007. Modelling of Gas Generation from the Barnett Shale. Fort Worth Basin, Texas.

Hood, A., Gutjahr, C.C.M., Heacock, R.L., 1975. Organic Metamorphism and Generation of Petroleum: American Association of Petroleum Geologists Bulletin, vol. 59, pp. 986–996.

Hunt, J.M., Lewan, M.D., Hennet, R.J.C., 1991. Modeling oil generation with time-temperature index graphs based on the Arrhenius equation. Am. Assoc. Petrol. Geol. Bull. 75 (4), 795–805.

Hunt, J.M., 1996. Petroleum Geochemistry and Geology. W.H. Freeman and Co., p. 742

Iqbal, M.W.A., Shah, S.I., 1980. A Guide to the Stratigraphy of Pakistan, vol. 53. Geological Survey of Pakistan.

Jarvie, D.M., 2012. Shale Resource Systems for Oil and Gas: Part 2—Shale-Oil Resource Systems.

Jarvie, D.M., Hill, R.J., Ruble, T.E., Pollastro, R.M., 2007. Unconventional shale-gas systems: the Mississippian Barnett Shale of north-central Texas as one model for thermogenic shale-gas assessment. AAPG Bull. 91 (4), 475–499.

Khan, M., Arif, M., Ali, N., Yaseen, M., 2016. Petrophysical parameters and modelling of Eocene reservoirs in the Qadirpur area, Central Indus Basin, Pakistan, implications from well log analysis. Arabian J. Geosci. 9, 425 (2016).

Klett, T.R., Schenk, C.J., Wandrey, C.J., Brownfield, M., Charpentier, R.R., Cook, T., Gautier, D.L., Pollastro, R.M., 2011. Assessment of Potential Shale Gas Resources of the Bombay, Cauvery, and Krishna–Godavari Provinces. USGS Fact Sheet, India, pp. 3131–3132.

Leite, E.P., Vidal, A.C., 2011. 3D porosity prediction from seismic inversion and neural networks. Comput. Geosci. 37 (8), 1174–1180.

Liu, L., Shang, X., Wang, P., Guo, Y., Wang, W., Wu, L., 2012. Estimation on organic carbon content of source rocks by logging evaluation method as exemplified by those of the 4th and 3rd members of the Shahejie Formation in Western Sag of Liaohe Oilfield. Chin. J. Geochem. 31 (4), 398–407.

Løseth, H., Wensaas, L., Gading, M., Duffaut, K., Springer, M., 2011. Can hydrocarbon source rocks be identified on seismic data? Geology 39 (12), 1167–1170.

Mavko, G., Jizba, D., 1990. Seismic P, and S-wave dispersion in saturated rocks. SEG Tech. Progr. Expand. Abstr. 783–786.

Mavko, G., Mukerji, T., Dvorkin, J., 2009. The Rock Physics Handbook: Tools for Seismic Analysis of Porous Media. Cambridge University Press, Cambridge, pp. 34–77.

Meyer, B.L., Nederlof, M.H., 1984. Identification of source on wireline logs by density/resistivity and sonic transit time/resistivity cross-plot. AAPG (Am. Assoc. Pet. Geol.) Bull. 68, 121–129.
Milan, G., Rodgers, M., 1993. Stratigraphic Evolution and Play Possibilities in the Middle Indus Area, Pakistan. SPE Pakistan Seminar. Islamabad January 19.
Myers, K.J., Jenkyns, K.F., 1992. Determining total organic carbon content from well-logs: an inter-comparison of GST data and anew density log method. In: Hurt, A., Griffiths, C.M., Worthington, P.F. (Eds.), Geological Application of Wire-Line Logs, second ed., vol. 65. Geological Society, London Special Publication, pp. 369–376.
Obert, L., Duvall, W., 1967. Rock Mechanics and the Design of Structures in Rock. Wiley, New York.
Opera, A., Alizadeh, B., Sarafdokht, H., Janbaz, M., Fouladvand, R., Heidarifard, M.H., 2013. Burial history reconstruction and thermal maturity modeling for the middle cretaceous–early miocene petroleum System, southern Dezful Embayment, SW Iran. Int. J. Coal Geol. 120, 1–14.
Passey, Q.R., Bohacs, K.M., Esch, W.H., Klimentidis, R., Sinha, S., 2010. From oil-prone source rock to gas-producing shale reservoir-geologic and petrophysical characterization of unconventional shale gas reservoirs. In: Society of Petroleum Engineers (SPE 13150): International Oil and Gas Conference and Exhibition 8-10 June, Beijing, China, pp. 1–29.
Passey, Q.R., Creaney, S., Kulla, J.B., Moretti, F.J., Stroud, J.D., 1990. A Practical Model for Organic Richness from Porosity and Resistivity Logs: AAPG Bulletin, vol. 74, pp. 1777–1794.
Philippi, G.T., 1965. On the depth, time and mechanism of petroleum generation: Geochemica et Cosmochimica Acta, vol. 29, pp. 1021–1049.
Raza, H.A., Ali, S.M., Ahmed, R., Ahmed, J., 1990. Petroleum geology of kirther sub–basin and part of kutch basin. Pak. Hydrocarb. Res. 2 (1), 29–73.
Rezaee, R., 2015. Fundamentals of Gas Shale Reservoirs. Wiley, Hoboken, pp. 191–245.
Rickman, R., Mullen, M.J., Petre, J.E., Grieser, W.V., Kundert, D., 2008. A Practical Use of Shale Petrophysics for Stimulation Design Optimization: All Shale Plays Are Not Clones of the Barnett Shale, vols. 1–11. Annual Technical Conference and Exhibition, Society of Petroleum Engineers (SPE), Denver, Colorado, USA.
Rider, M., 2002. The Geological Interpretation of Well Logs, second ed., p. P291
Robert, P., 1988. Organic Metamorphism and Geothermal History. Elf-Aquitane and Reidel Publishing, Dordrecht, p. 311.
Robison, C.R., Smith, M.A., Royle, R.A., 1999. Organic facies in Cretaceous and Jurassic hydrocarbon source rocks, Southern Indus basin, Pakistan. Int. J. Coal Geol. 39, 205–225.
Rybach, L., 1986. Amount and significance of radioactive heat sources in sediments. In: Burrus, J. (Ed.), Collection Colloques et Seminares 44, Thermal Modelling of sedimentary Basins Peris. Paris ed: Technip, 1986, pp. 311–322.
Schmoker, J.W., 1979. Determination of organic content of Applachian Devonian shales from formation-density logs. AAPG (Am. Assoc. Pet. Geol.) Bull. 63, 1504–1537.
Schmoker, J.W., 1981. Organic-matter Content of Appalachian Devonian Shales Determined by Use of Wire-Line Logs: Summary of Work Done 1976–1980. Geological Survey, Reston, pp. 81–181.
Schwarzkopf, T.A., 1992. Source rock potential (TOC + hydrogen index) evaluation by integrating well log and geochemical data. Org. Geochem. 19 (4), 545–555.
Scotese, C.R., Gahagan, L.M., Larson, R.L., 1988. Plate tectonic reconstructions of the cretaceous and cenozoic ocean basins. Tectonophysics 155, 27–48.
Sheikh, N., Giao, P.H., 2017. Evaluation of shale gas potential in the lower cretaceous Sembar formation, the southern Indus Basin, Pakistan. J. Nat. Gas Sci. Eng. 44, 162–176.
Sheriff, R.E., 1984. Encyclopedic Dictionary of Exploration Geophysics: Soc. Expl. Geophys.
Shrestha, N., Chilkoor, G., Wilder, J., Gadhamshetty, V., Stone, J.J., 2017. Potential water resource impacts of hydraulic fracturing from unconventional oil production in the Bakken shale. Water Res. 108, 1–24.
Sohail, G.M., Hawkes, C.D., Yasin, Q., 2020. An integrated petrophysical and geomechanical characterization of Sembar Shale in the Lower Indus Basin, Pakistan, using well logs and seismic data. J. Nat. Gas Sci. Eng. 78, 103327.
Sunjay, 2011. Shale Gas: an Unconventional Reservoir. Recovery—2011 CSPG CSEG CWLS Convention, pp. 1–4.
Tissot, B., Welte, D.H., 1978. Petroleum Formation and Occurrence: A New Approach to Oil and Gas Exploration. Springer-Velag Berlin.
Wandrey, C.J., Law, B.E., Shah, A.H., 2004. Sembar Goru/Ghazij Composite Total Petroleum System, Indus and Sulaiman-Kirther Geological Province, Pakistan and India. USGS Bulletin, pp. 1–23.
Wood, D.A., 1988. Relationships between thermal maturity indices calculated using Arrhenius equation and Lopatin method: implications for petroleum exploration. Am. Assoc. Petrol. Geol. Bull. 72 (2), 115–134.
Wood, D.A., 2017. Reestablishing the merits of thermal maturity and petroleum generation multi-dimensional modeling with an Arrhenius equation using a single activation energy. J. Earth Sci. 28 (5), 804–834.
Yu, H., Rezaee, R., Wang, Z., Han, T., Zhang, Y., Arif, M., Johnson, L., 2017. A new method for TOC estimation in tight shale gas reservoirs. Int. J. Coal Geol. 179, 269–277.
Zhang, D.C., Ranjith, P.G., Perera, M.S.A., 2016. The brittleness indices used in rock mechanics and their application in shale hydraulic fracturing: a review. J. Petrol. Sci. Eng. 143, 158–170.